Chemical Geology 511 (2019) 314–341

Contents lists available at ScienceDirect

Chemical Geology

journal homepage: www.elsevier.com/locate/chemgeo

Cycles of trace elements and isotopes in the ocean - GEOTRACES and beyond

The shelf-to-basin iron shuttle in the Black Sea revisited☆

W.K. Lenstra[a,*], M. Hermans[a], M.J.M. Séguret[a], R. Witbaard[b], T. Behrends[a], N. Dijkstra[a], N.A.G.M. van Helmond[a], P. Kraal[a,c], P. Laan[c], M.J.A. Rijkenberg[c], S. Severmann[d], A. Teacă[e], C.P. Slomp[a]

[a] Department of Earth Sciences - Geochemistry, Utrecht University, PO Box 80021, Utrecht, 3508 TA, The Netherlands
[b] Department of Estuarine and Delta Systems, NIOZ, Netherlands Institute for Sea Research and Utrecht University, PO Box 140, Yerseke 4400 AC, The Netherlands
[c] Department of Ocean Systems, NIOZ, Netherlands Institute for Sea Research and Utrecht University, PO Box 59, Den Burg 1790 AB, Texel, The Netherlands
[d] Department of Marine and Coastal Science, Rutgers, The State University of New Jersey, New Brunswick, NJ 08901-8521, USA
[e] National Research and Development Institute for Marine Geology and Geoecology - NIRD GeoEcoMar, Bucharest, Romania

ARTICLE INFO

Editor: Michael E. B

Keywords:
Iron
Lateral transport
Continental shelf sediment
Organic matter
Bioirrigation
GEOTRACES

ABSTRACT

Continental shelf sediments are a major source of iron (Fe) for phytoplankton in surface waters. In this study, we investigate the mechanisms that control release of Fe from shelf sediments and its lateral transport ("shuttling") in oxic and hypoxic waters on the northwestern Black Sea shelf. We find that at two coastal stations near the outflow of the Danube river high input of organic matter drives strong reductive dissolution of Fe(oxyhydr) oxides (henceforth termed Fe oxides) in surface sediments, supporting high rates of Fe release to oxygenated bottom waters (~ 0.36 mmol m^{-2} d^{-1}). We suggest that bioirrigation plays a key role in the release of Fe from these sediments. At four stations further offshore organic matter deposition is lower resulting in limited mobilization of Fe^{2+} in the sediment and low benthic fluxes of Fe (< 0.07 mmol m^{-2} d^{-1}). Lateral transport of Fe from the coastal zone towards the deep basin mostly takes place in colloidal and/or particulate form (> 0.2 μm) in the lower part of the water column, likely through repeated deposition and resuspension of Fe oxides from surface sediments. Using synchrotron-based X-ray spectroscopy and sequential chemical extractions, we demonstrate that the suspended matter and surface sediments are enriched in easily reducible Fe oxides (mostly ferrihydrite) and Fe associated with clay. The mobilization of Fe in the coastal zone and subsequent lateral transport of these Fe-bearing particles results in higher ratios of Fe/Al in surface sediments at outer shelf stations (ca. 1.2 to 2 wt.% $wt.\%^{-1}$) than at coastal stations (ca. 0.5 to 0.9 wt.% $wt.\%^{-1}$). However, below the sediment surface layer Fe/Al ratios are similar at all stations indicating limited burial of the laterally transported Fe. Our results highlight the critical role of organic matter input, associated biological activity and riverine Fe input as drivers of Fe shuttling on continental shelves. We also show that in shelf areas where sediments receive low inputs of organic matter, physical transport controls the ultimate fate of the shuttled Fe.

This article is part of a special issue entitled: "Cycles of trace elements and isotopes in the ocean - GEOTRACES and beyond" - edited by Tim M. Conway, Tristan Horner, Yves Plancherel, and Aridane G. González.

1. Introduction

Iron (Fe) is an essential micronutrient that can limit the growth of phytoplankton in the ocean (Martin and Fitzwater, 1988; Moore et al., 2013; Tagliabue et al., 2017). Release of Fe from continental shelf sediments is a key source of both dissolved and particulate Fe in offshore areas (Canfield et al., 1996; Wijsman et al., 2001a; Raiswell and Canfield, 2012). This release and lateral transport of Fe, which is termed "Fe shuttling", is a complex function of a range of factors such as organic matter input, bottom water oxygen (O_2) and biological and physical transport processes (Elrod et al., 2004; Dale et al., 2015). Temporal variations in Fe shuttling can be recorded in deep basin sediments overlain by anoxic and sulfidic (euxinic) waters adjacent to continental shelves (Lyons and Severmann, 2006). Mechanistic insight in Fe shuttling on continental shelves is critical for our understanding of variations in Fe availability in the ocean due to natural and human-

☆ This article is part of a special issue entitled: "Cycles of trace elements and isotopes in the ocean - GEOTRACES and beyond" - edited by Tim M. Conway, Tristan Horner, Yves Plancherel, and Aridane G. González.

* Corresponding author.
E-mail address: w.k.lenstra@uu.nl (W.K. Lenstra).

https://doi.org/10.1016/j.chemgeo.2018.10.024
Received 26 April 2018; Received in revised form 3 October 2018; Accepted 27 October 2018
Available online 08 December 2018

induced eutrophication and de-oxygenation (Diaz and Rosenberg, 2008; Scholz et al., 2014a).

Mobilization of ferrous iron (Fe^{2+}) in shelf sediments is highly dependent on the input of organic matter (Elrod et al., 2004). Degradation of organic matter drives the reductive dissolution of ferric (Fe(III)) (oxyhydr)oxides (henceforth termed Fe oxides) and subsequent release of Fe^{2+} into porewaters (Lovley and Phillips, 1987; Canfield, 1989). Part of this Fe^{2+} can diffuse upwards where it may re-oxidize and form Fe oxides by reaction with O_2, nitrate, nitrite and/or manganese oxides near the sediment-water interface (Postma, 1985; Kappler et al., 2005; Scholz et al., 2016; Robertson et al., 2016). In sediments where sulfide is abundant, Fe^{2+} can precipitate as Fe sulfide (Berner, 1970, 1984). Escape of Fe^{2+} to the overlying water through diffusion is most pronounced under oxygen-depleted but non-sulfidic bottom water conditions (Slomp et al., 1997; Homoky et al., 2011). Evidence for such a "redox window" in which release of Fe from shelf sediments is enhanced is available from both direct measurements of benthic fluxes (Pakhomova et al., 2007; Severmann et al., 2010; Noffke et al., 2012) and the geological record (i.e. Scholz et al., 2014a; Lenz et al., 2015).

The presence of macrofauna can enhance the release of Fe from sediments through bioturbation and bioirrigation (Berelson et al., 2003; Elrod et al., 2004; Severmann et al., 2010). Bioturbation is a key driver of downward transport of Fe oxides and organic matter, and thereby stimulates Fe mobilization in sediments (Canfield et al., 1993; Aller, 1994). Bioirrigation, the ventilation of burrows by macrofauna, increases the exchange of solutes between porewater and the overlying water and can enhance Fe^{2+} release from sediments. However, given that bioirrigation also enhances the input of O_2 into the sediment (Aller, 1982; Aller and Aller, 1998) and that the oxidation kinetics of Fe^{2+} are fast at circumneutral pH (Millero et al., 1987; Nealson, 1997), bioirrigation can also lead to oxidation of Fe^{2+} inside burrows and formation of colloidal or nanoparticulate ferric iron particles that can remain in suspension (particle size mostly between 0.02 and 0.2 μm, Raiswell and Canfield, 2012). Upon flushing of burrows, some of this colloidal and nanoparticulate Fe might be released to the overlying water.

Dissolved Fe^{2+} that escapes from the sediment can precipitate as Fe oxides or, if it is complexed with organic ligands, can remain in solution at nanomolar levels (Gledhill and van den Berg, 1994; Rue and Bruland, 1995; Klar et al., 2017). While larger Fe oxide particles will typically sink directly and settle at the sediment-water interface, a significant proportion of the dissolved, colloidal and nanoparticulate Fe may be transported laterally through currents (Cullen et al., 2009; Noble et al., 2012). On continental shelves, repeated deposition and remobilization or resuspension of part of this Fe may occur during this lateral transfer. The characteristic mineralogy and isotope composition from shelf-derived Fe has been used to trace it over hundreds of kilometers offshore (Lam et al., 2012; Conway and John, 2014). In some cases, Fe may also be retained on the shelf (e.g. Hong and Kester, 1986; Scholz et al., 2014b), likely due to settling of Fe-bearing particulate matter.

In the Black Sea, the transfer of Fe from the continental shelf to offshore regions is recorded in the adjacent deep basin sediments. This is the result of efficient trapping of incoming Fe as Fe sulfides in the anoxic and sulfidic (euxinic) water column that is characteristic for the off shelf waters in the Black Sea below 150 m (e.g. Wijsman et al., 2001a; Raiswell and Canfield, 2012). Records of Fe/Al for the Holocene show major variations in Fe input to the deep basin on time scales of millennia, that have been attributed to variations in the efficiency of the shelf to basin Fe shuttle linked to the position of the chemocline (Eckert et al., 2013). In this scenario, release of Fe from slope or shelf sediments overlain by suboxic waters in the chemocline controls the efficiency of the Fe shuttle. The sediment area underlying the present-day chemocline is relatively small, however, and the Fe supply to the deep basin can only be maintained if replenished by Fe input from the wider shelf (Anderson and Raiswell, 2004; Lyons and Severmann, 2006) or from rivers. Given that the waters overlying the Black Sea shelf are currently mostly oxygenated, this implies a need for significant transport of Fe through an oxic water column ("oxic shuttling of Fe"; Raiswell and Canfield, 2012). While coastal sediments have been suggested to act as the major source of Fe to the deep basin based on sediment Fe analyses (Wijsman et al., 2001a), it is not well understood where and how Fe is released from Black Sea shelf sediments, whether oxic shuttling involves recycling of Fe from sediments over the whole shelf, and in what form the Fe is transported.

In this study, we assess the dynamics of Fe in the sediment and water column at seven stations along a water depth transect in the northwestern Black Sea. By combining *in-situ* benthic flux measurements and a range of porewater, sediment and water column analyses, we were able to identify the areas of the shelf where Fe is released from the sediment and in which form Fe is transported across the shelf. We also explore the role of bioirrigation in sedimentary Fe release by assessing the macrofaunal abundance and activity. We find that organic-rich, bioirrigated coastal sediments are a key source of Fe in oxic waters overlying the northwestern shelf of the Black Sea and that transport of Fe on the shelf is dominated by physical transport of a mixture of Fe oxides and Fe associated with clay (clay-Fe).

2. Methods

2.1. Study area and sampling

Our study sites are located along a transect on the northwestern Black Sea shelf, with water depths ranging from 27 to 180 m (Fig. 1; Table 1). Water column and sediment samples were collected at seven stations during a cruise with *R/V* Pelagia in September 2015. Two stations were near the mouth of the Danube river, two stations were on the open shelf and three were on the shelf edge (Table 1). The northwestern Black Sea shelf covers an area of 70,000 km^2 (Wijsman et al., 1999). In the Black Sea, oxic surface waters are separated from the euxinic deep basin by a suboxic chemocline at ~150 m water depth (Arthur and Dean, 1998; Coolen et al., 2009). Depth profiles of conductivity, temperature, density and dissolved O_2 were obtained with a CTD profiler equipped with an O_2 sensor (SBE43) on a titanium frame. Water samples were collected using ultra-trace metal clean PVDF samplers attached to the same frame (Rijkenberg et al., 2015), deployed with a Kevlar hydrowire (De Baar et al., 2008; Rijkenberg et al., 2014). Sediment cores were collected with an Oktopus multicorer (inner diameter: 10 cm) using polycarbonate tubes of 60 cm length. Only sediments with a minimum of 20 cm overlying water and an intact sediment surface were processed further. At all stations, two bottom water samples were taken directly after core retrieval. *In-situ* benthic flux measurements were carried out with an Albex lander (Witbaard et al., 2000) at all stations except station 5.

2.2. Water column analyses

Unfiltered samples for total dissolvable Fe (henceforth termed "total Fe") were taken from the PVDF samplers using acid-washed LDPE tubing. Samples for dissolved Fe were obtained using a 0.2 μm Sartobran 300 cartridge (Sartorius), which was pre-filtered with 0.5 L of ambient seawater. In both cases, nitrogen pressure was applied at the top of the sampler and the samples were collected in acid-washed 60 mL LDPE bottles (Nalgene), filled to the shoulder of the bottle. Samples were acidified to pH 1.8 by adding 120 μL of distilled 10 M HCl to 60 mL of sample. Samples were stored at 4°C until analysis.

The concentration of Fe was determined by flow injection chemiluminescence with pre-concentration detection at Utrecht University (Klunder et al., 2011; Rijkenberg et al., 2014). All samples per station were analyzed in triplicate in the same run. We ensured that all the Fe was in the Fe^{3+} form by adding 0.1% hydrogen peroxide more than 12 h before analysis. Each sample was loaded on a chelating iminodiacetic acid (IDA), Toyopearl, AFChelate column for 25 s(high concentration; i.e. 2–25 nM) or 90 s(low concentration; i.e. 0–2 nM),

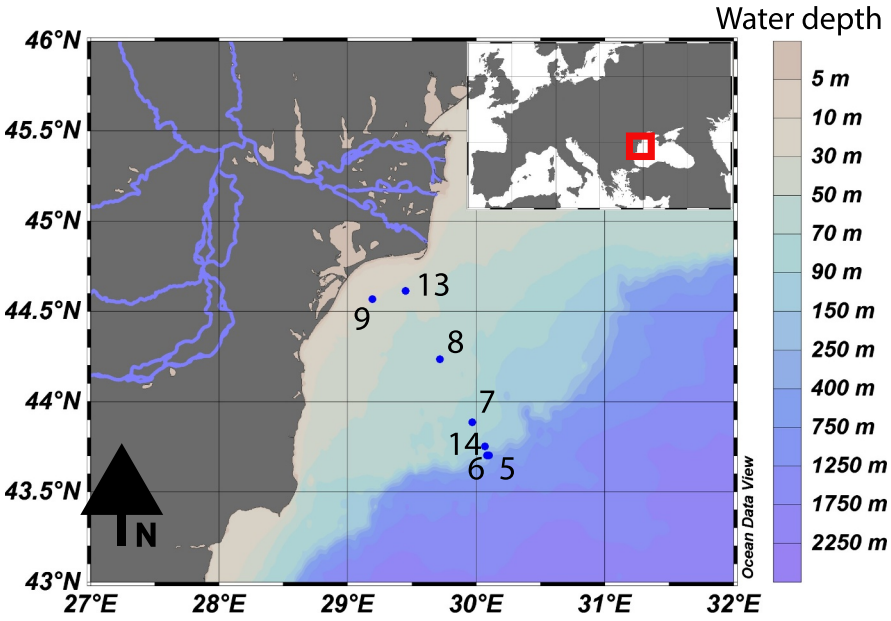

Fig. 1. Locations of the 7 stations sampled on the northwestern Black Sea shelf in September 2015. Figure drawn using Ocean Data View (Schlitzer, 2015).

Table 1
Coordinates, water depth, bottom water temperature and salinity at the 7 stations sampled on the northwestern Black Sea shelf. Unit mbss is meters below sea surface.

Station	Latitude N	Longitude E	Depth mbss	Temperature °C	Salinity
9 (coast)	44°34.9′	29°11.4′	27	13.3	17.9
13 (coast)	44°36.4′	29°27.4′	44	9.2	18.1
8 (open shelf)	44°14.7′	29°43.4′	65	8.2	18.2
7 (open shelf)	43°53.8′	29°58.6′	78	8.5	18.7
14 (shelf edge)	43°45.9′	29°11.4′	114	8.4	19.5
6 (shelf edge)	43°42.8′	30°05.1′	130	8.5	20.0
5 (shelf edge)	43°42.6′	30°06.1′	180	8.6	21.2

followed by a rinse of 60 s with ultrapure de-ionized water (< 18.2 MΩ) and elution for 110 s with 0.4 M suprapur HCl. All reagents were prepared with suprapur grade chemicals and ultrapure de-ionized water. The blank of acidified ultrapure water (pH = 1.8) was 20 ± 17 pM (n = 512). The average limit of detection, calculated as the standard deviation of the blanks, multiplied by 3, was 24 ± 18 pM. The accuracy of the system was checked daily using GEOTRACES reference seawater. For SAFe (D1), we measured an average value of 0.69 ± 0.03 nM, consistent with the community consensus value of 0.67 ± 0.04 nM (Johnson et al., 2007 and www.geotraces.org (2013)).

Suspended matter was collected through *in-situ* pumping for 1–4 h at 2 to 4 water depths per station (Table A.1) using four McLane pumps (3x WTS-LV, 1x WTS-LV Dual Filter). After retrieval of the pumps, water around filters (Supor, 0.8 µm, 142 mm diameter) was removed by vacuum pumping and the filters were placed in petri-dishes, sealed in plastic bags and stored at − 20°C. The forms of Fe in the suspended matter were determined on a quarter of every filter in a 4-step sequential extraction procedure targeting the following phases (Table 2): (1) ferrihydrite, (2) easily reducible Fe(III) and Fe(II) minerals, (3) reducible (crystalline) Fe oxides and (4) magnetite. Step (1) was taken from Raiswell et al. (2010). Steps (2) –(4) are based on Poulton and Canfield (2005) and Claff et al. (2010) as described by Kraal et al. (2017). Total Fe in the extraction solutions was determined colorimetrically using the 1,10-phenanthroline method (APHA, 2005) after reduction of Fe(III) to Fe(II) by 0.4 M hydroxylamine hydrochloride. In the 1 M HCl solutions (step 2), both Fe(II) and total Fe were measured and Fe(III) was calculated by extracting the Fe(II) pool from total Fe.

2.3. Porewater analyses

At each station, one sediment core was sliced into intervals of 0.5 to 3 cm under a nitrogen atmosphere at bottom water temperature (Table 1). Each slice was divided over a pre-weighed glass vial and a 50 mL centrifuge tube. The glass vials were stored under a nitrogen atmosphere at − 20°C for solid phase analyses onshore. The 50 mL centrifuge tubes were centrifuged on board at 4500 rpm for 20 min to extract porewater. Porewater was filtered under a nitrogen atmosphere through 0.45 µm pore size filters to determine total dissolved Fe. At station 9, porewater was also filtered through 0.2 and 0.02 µm pore size filters to differentiate between colloidal/nanoparticulate (0.02 –0.2 µm) and aqueous (< 0.02 µm; (Boyd and Ellwood, 2010; Homoky et al., 2011; Raiswell and Canfield, 2012)) Fe. All samples were acidified with 10 µL 10 M suprapur HCl per mL of sample and stored at 4°C prior to analysis. Total dissolved Fe at all stations was analyzed by inductively coupled plasma optical emission spectroscopy (ICP-OES; Spectro Arcos). The samples for the < 0.02, < 0.2 and < 0.45 µm filter fractions for station 9 were measured colorimetrically using the 1,10-phenanthroline method (APHA, 2005). The ICP-OES and colorimetric results for total dissolved Fe fraction (< 0.45 µm) at station 9 were similar (Fig. A.1). Concentrations of ammonium (NH_4^+), sulphate (SO_4^{2-}) and sulfide (H_2S) were determined as described in Kraal et al. (2017)).

At stations 9 and 13, high-resolution depth profiles of dissolved O_2 were obtained in a separate sediment core directly after retrieval using microelectrodes (50 µm resolution) and a 2D-micromanipulator using a 2-point calibration with 100% O_2 saturated and nitrogen purged artificial seawater (Unisense A.S., Denmark). Diffusive fluxes of O_2 and Fe^{2+} (J in mmol m^{-2} d^{-1}) across the sediment-water interface were calculated using Fick's first law of diffusion (Eq. (1)):

$$J = -\varphi^* D_s^* \frac{dC}{dz} \quad (1)$$

where φ is porosity, D_s is the molecular diffusion coefficient for Fe^{2+}, corrected for tortuosity in the porous medium (Boudreau, 1996), and dC/dz is the concentration gradient between the top layer of the sediment and the bottom water concentration. The molecular diffusion coefficient D_s for the ambient salinity, pressure and temperature at each

Table 2
Sequential extraction procedure for Fe as performed on suspended matter (steps 1 to 4) and sediment samples (steps 2 to 4) based on Poulton and Canfield (2005) and Claff et al. (2010). A separate extraction was carried out to extract FeS_2 after removal of FeS with 6 M HCl for 24 h and elemental sulfur with methanol for 16 h, followed by an acetone rinse for 20 min according to Burton et al. (2006, 2008). The sum of extracted Fe in the different steps is defined as highly reactive Fe.

Step	Extractant	Time (hours)	Target phase	Term
1	0.17 M sodium citrate, 0.6 M sodium bicarbonate and 0.057 M ascorbic acid (pH 7.5)	24	Ferrihydrite	Ferrihydrite
2	1 M HCl	4	Easily reducible Fe oxides Fe carbonates and FeS	Fe_{ox1} Fe(II)
3	50 g L^{-1} sodium dithionite solution buffered to pH 4.8 with 0.35 M acetic acid/0.2 M sodium citrate	4	Reducible (crystalline) Fe oxides	Fe_{ox2}
4	0.2 M ammonium oxalate/0.17 M oxalic acid (pH 3.2)	6	Magnetite	Fe_{mag}
	500 g L^{-1} chromous chloride in 10 M HCl	48	FeS_2	FeS_2

* Magnetite may also be extracted in this step (Henkel et al., 2016).

station was calculated using the R package CRAN: marelac (Soetaert et al., 2010), which implements the constitutive relations listed in Boudreau (1997).

2.4. Solid phase analyses

All sediments were freeze-dried and the porosity was determined from the weight loss upon freeze drying. Freeze-dried sediments were ground in an agate mortar inside an argon filled glovebox and separated into various subsamples. To determine the total elemental concentrations, ca. 125 mg of sediment was digested in 2.5 ml mixed acid (HNO_3:$HClO^-4$; 2:3) and 2.5 ml 40% HF at 90°C. After fuming off the acids, the residue was redissolved in 1 M HNO_3. The solutions were subsequently analyzed for total Fe, S and aluminum (Al) on an ICP-OES. The analytical uncertainty based on duplicates was 5% for Fe, 7% for S and 5% for Al. A second subsample of circa 300 mg was decalcified with 2 wash steps of 1 M HCl (Van Santvoort et al., 2002) and subsequently dried, powdered and analyzed for carbon (C) using an elemental analyzer (Fisons Instruments model NA 1500 NCS). Organic C contents were determined after correction for the weight loss following decalcification. A third subsample of circa 50 mg was subjected to steps (2) –(4) of the sequential extraction procedure for Fe (Table 2). Pyrite was determined in a separate extraction as chromium reducible sulfur (CRS) from which FeS and elemental sulfur first were removed (only at stations 9, 13, 8; Table 2; Burton et al., 2006, 2008). The analytical uncertainty based on duplicates was 3%, and 3.5% for steps (2) to (4), respectively, and 8% for CRS.

2.5. X-ray spectroscopy: Fe k-edge XANES and EXAFS

Freeze-dried and finely-ground sediment samples from stations 9, 13, 8, 7, 14, 6 and 5 and suspended matter samples (collected through *in-situ* pumping) from the same stations were analyzed by X-ray absorption spectroscopy (XAS) analysis at the Dutch-Belgian beamline (DUBBLE, BM26a) at the European Synchrotron Radiation Facility (ESRF) in Grenoble (France). A description of the set-up and the optics of the beamline is provided by Borsboom et al. (1998) and Nikitenko et al. (2008).

The powdered sediment samples were compressed to a pellet and measured in transmission mode at room temperature. The amount of sediment sample per pellet was optimized in view of minimizing total adsorption and maximizing the step height of the Fe edge. Suspended material was measured in fluorescence mode using a 9 element Ge detector. The energy was calibrated using Fe(0) foil by assigning the energy of 7112 eV to the maximum slope of the absorption edge. The software Athena (Ravel and Newville, 2005) was used for averaging spectra, normalization, background subtraction as well as for linear combination fitting. For X-ray absorption near edge structure (XANES) spectra, the energy range between 7100 and 7180 eV, and for the k^2 weighted extended x-ray absorption fine structure (EXAFS) spectra the k-range between 1 and 9 $Å^{-1}$ was used in the linear combination fitting.

XANES and EXAFS spectra collected from the powdered sediments were compared to those of a variety of reference materials. The library of reference materials used for this comparison consists of a wide range of Fe containing minerals and includes various Fe oxides, siderite, vivianite, FeS, pyrite, and several silicates such as clay minerals and biotite (Fig. A.2). Based on this pre-screening, three reference materials were identified of which the combination of XANES and EXAFS spectra gave the best reproduction of spectra from the bulk sediment samples. These were Fithian illite, which was treated with dithionite to remove Fe oxides, 6-line ferrihydrite and pyrite (Schwertmann and Cornell, 2007). Based on electrochemical analysis, about 20% of the structurally bound Fe in the illite is in the form of Fe(II) (Hoving et al., 2017).

For the sediment samples, only spectra collected in transmission mode with a step height larger than 0.1 were included in the analysis. As a consequence, the spectra for station 7 were excluded. The bulk XAS measurements of suspended material only yielded spectra with sufficient quality at stations 9 and 13.

The suspended matter from stations 9 and 13 was analyzed at the X-ray microscopy beamline ID21 (Salomé et al., 2013) at the ESRF. The dimensions of the beam were about 400 nm vertically and 800 nm horizontally. μ-XRF mapping was performed at an energy of 7200 eV. The spatial distribution of the elements Fe and potassium (K) was determined and Fe-XANES spectra were collected at various spots on the sample.

2.6. In-situ benthic flux of Fe and O_2 and macrofaunal density

Benthic O_2 uptake and fluxes of total Fe across the sediment-water interface were determined *in-situ* with a benthic lander, equipped with three chambers made of the inert plastic delron, each with a surface area of 144 cm^2 and volume between 1.3 and 1.8 L of water (Witbaard et al., 2000). Two or three of the chambers were equipped with dissolved O_2 optodes (JFE Advantech; Fig. A.3). During the incubation, water samples were taken simultaneously with 30 mL plastic syringes connected to inlet ports inside and outside the incubation chamber after 2, 4, 7, 10 and 13 h. Each time a water sample was taken from the chamber, an equivalent volume of surrounding bottom water was allowed to enter the chamber. At the end of the deployment, the chambers were closed at the bottom allowing the upper ~12 cm of sediment to be collected upon retrieval of the lander. The sediment from each chamber was sieved over a 0.5 mm mesh size. Macrofauna was collected and stored in 4% formaldehyde in plastic jars (Eleftheriou and McIntyre, 2007) until determination of the species and number of macrofauna. At station 5, only samples for macrofauna were collected because the incubation chambers were inserted too deep into the soft sediment and the volume of water in the chambers was not sufficient

for sampling. Upon lander retrieval from the seafloor the water samples were directly transferred to a temperature controlled laboratory maintained at *in-situ* temperature, acidified with 10 µL 10 M suprapur HCl per mL of sample and stored at 4°C. Total Fe in the syringe samples was determined through flow injection chemiluminescence as described above. Fluxes of Fe across the sediment-water interface were determined by fitting a linear regression to the concentration time series from each chamber (after correction for the dilution with the bottom water at each sampling interval). Only regressions with $R^2 > 0.3$ were considered, following Friedrich et al. (2002) (Fig. A.4). Calculated Fe fluxes for the different incubation chambers were averaged for each station. Oxygen uptake was determined by fitting a linear regression line through all data points at all stations except for station 9 where only data collected in the first two hours were used due to a change in slope. To assess the potential consequences for Fe release, the benthic Fe release based on the first three time points was also determined (Table 5).

2.7. Bioirrigation rates

At stations 9 and 13, a sediment core was incubated with the inert tracer bromide to determine bioirrigation rates (Martin and Banta, 1992). Directly after core retrieval, the volume of the overlying water was adjusted to 550 mL and a concentrated bromide solution was added to the overlying water to achieve a concentration of ca. 2.5 mM. During a two-day incubation at *in-situ* temperature, the overlying water was kept saturated with O_2 and well-mixed by bubbling with air. After incubation, the sediment was sliced into intervals of 0.5 to 4 cm and centrifuged for 20 min at 4500 rpm. After centrifugation, the supernatant was filtered (0.45 µm) and stored at 4°C. Bromide concentrations were determined with ion chromatography. Rates of bioirrigation were calculated assuming a 1-D, nonlocal exchange function (Appendix A.1; Emerson et al., 1984; Boudreau, 1984).

3. Results

3.1. General station characteristics

Bottom water temperature and salinity at the 7 stations ranged from 8.2 to 13.3°C and 17.9 to 21.2, respectively (Table 1). Bottom water O_2 was the highest at the coastal station 13 at 209 µmol L^{-1} O_2 and decreased to 5 µmol L^{-1} at station 5 at the shelf edge (Table 3; Fig. 2A). The coastal station 9 had a relatively low O_2 concentration of 92 µmol L^{-1}. *In-situ* measured O_2 uptake was the highest at coastal stations 9 and 13, at values of 25.8 and 17.8 mmol m^{-2} d^{-1}, respectively, and decreased offshore (Fig. 2B). Oxygen penetration depths in the sediment at stations 9 and 13 were 2.25 and 1.65 mm, respectively (Table 3; Fig. A.5). Calculated diffusive fluxes of O_2 were a factor 2 lower than measured O_2 fluxes (Table 3). Organic carbon contents in the surface sediments (0–0.5 cm) at the coastal stations 9 and 13 ranged from 1.8 to nearly 2.9 wt. % and were distinctly higher than those in offshore areas, where values ranged from 0.5 to 1.3 wt. % (Table 3). Similarly NH_4^+ concentrations were higher and there was less of a decline in porewater SO_4^{2-} with depth at the coastal sites than at the shelf and shelf edge stations. Concentrations of H_2S were very low in the upper 5 cm of the sediment at all sites except station 5 (Fig. A.6).

3.2. Macrofaunal density and activity

The macrofaunal density was the highest at the coastal stations, where on average ca. 6000 to 9000 individuals per m^2 were observed (Table 4; Fig. 2C). The macrofaunal density decreased towards the shelf edge. At station 9 bivalves were the most abundant macrofaunal species while at station 13 worms were the most abundant (Table 4). No living macrofauna were found at station 5. Results of bromide incubations suggest bioirrigation activity down to a depth of 17 and 8 cm depth at stations 9 and 13, respectively (Fig. A.7). Results of 1D-modeling of the bromide profiles suggest a depth-averaged non-local transport coefficient (α) in this bioirrigated layer of 0.41 d^{-1} at station 9 and 0.21 d^{-1} at station 13.

3.3. Water column Fe profiles

Surface waters were slightly enriched in total Fe at stations 8, 14, 6 and 5 (Fig. 3). At all stations, concentrations of dissolved and total Fe were elevated in the lower part of the water column. Dissolved and total Fe concentrations in the deeper water column decrease from the coast to the shelf edge (up to 1850 nM total Fe at station 9 versus ca. 20 nM total Fe at station 6). A similar offshore trend in total Fe is seen in bottom water taken during lander incubation (average of 2050 nM at station 9 to 290 nM at station 6 (Tables S.9 –S.14). At station 5, dissolved and total Fe increased rapidly below 150 m depth because of sampling of the chemocline in the deep basin (e.g. Kraal et al., 2017). At this station, particulate Fe additionally shows a maximum between 100 and 120 m water depth.

3.4. Benthic exchange and porewater profiles of Fe

In-situ measured benthic fluxes of total Fe towards the overlying water were the highest near the coast, with average values of 0.34 and 0.38 mmol m^{-2} d^{-1} at stations 9 and 13, respectively (Fig. 3B; Table 5; mean R^2 for all chambers: 0.84). At the open shelf and shelf edge stations, in contrast, average Fe fluxes were below 0.07 mmol m^{-2} d^{-1} and at station 6 an Fe flux into the sediment of ~0.2 mmol m^{-2} d^{-1} was observed. At station 7 no flux of Fe was detected. Porewater Fe profiles show a distinct subsurface maximum at all stations, which is indicative of release of Fe to the porewater (Fig. 3C). Dissolved Fe concentrations were an order of magnitude higher at the coastal stations 9 and 13 than at the open shelf and shelf edge stations. Accumulation of dissolved Fe was the strongest and occurred closest to the sediment-water interface at these coastal stations. At station 9, on average 70% of the dissolved Fe in the porewater (< 0.45 µm) was

Table 3
Key station characteristics: organic carbon contents in the surface sediment (0–0.5 cm), O_2 concentrations in the bottom water as determined with an O_2 sensor (SBE43) attached to the CTD frame, *in-situ* O_2 uptake as determined with chamber incubations, O_2 penetration depth in the sediment (mm) from microprofiles (Fig. A.5), calculated diffusive flux of O_2, and macrofaunal abundance (individuals m^{-2}). n.a.: not available.

Station	Organic C wt.%	O_2 Bottom water µmol L^{-1}	O_2 uptake mmol m^{-2} d^{-1}	O_2 penetration depth mm	O_2 diffusive flux mmol m^{-2} d^{-1}
9 (coast)	1.8	92	25.8 ± 1.77	2.25	13.0
13 (coast)	2.9	209	17.8 ± 2.8	1.65	9.4
8 (open shelf)	0.78	197	8.1 ± 3.4	n.a.	n.a.
7 (open shelf)	0.54	155	3.7 ± 1.4	n.a.	n.a.
14 (shelf edge)	1.25	93	1.6 ± 0.1	n.a.	n.a.
6 (shelf edge)	0.91	27	0.4 ± 0.02	n.a.	n.a.
5 (shelf edge)	n.a.	5	n.a.	n.a.	n.a.

Table 4
Abundance of macrofauna present in benthic lander incubation chambers (ind m^{-2}). Macrofaunal species are divided over three main groups: worms, mollusca and arthropoda. At station 5 no living macrofauna was found.

	Station 9			Station 13			Station 8			Station 7			Station 14			Station 6		
Lander chamber	1	2	3	1	2	3	1	2	3	1	2	3	1	2	3	1	2	3
Worms	417	1736	1597	6041	5208	8055	833	3472	1805	3056	2083	1389	1042	139	486	625	417	139
Fraction of polychaetes	1	0.96	0.65	0.78	0.7	0.67	0.5	0.82	0.8	1	0.93	0.9	1	1	1	0	0	0
Mollusca	3333	4097	7152	2083	2361	1944	0	2778	1458	3889	694	139	1389	417	2083	0	0	0
Arthropoda	69	69	69	278	208	69	347	2847	2569	486	486	833	0	69	69	0	0	0
Total	3819	5902	8818	8402	7777	10068	1180	9097	5832	7431	3263	2361	2431	625	2638	625	417	139

Table 5
In-situ measured and calculated diffusive benthic Fe fluxes. *In-situ* fluxes are averages for three incubation chambers. n.a.: not available. At station 7 a zero flux was determined; no measurement was carried out at station 5.

Station	Measured *in-situ* flux mmol m^{-2} d^{-1}	Calculated diffusive flux mmol m^{-2} d^{-1}
9	0.34 ± 0.12 *(0.11 ± 0.012)	2.23
13	0.38 ± 0.3	0.36
8	0.037 ± 0.01	−0.04
7	0	0
14	0.068	0
6	−0.19 ± 0.07	0.01
5	n.a.	0.001

* Benthic Fe release based on first three points in time (Fig. A.4). Although we did not see a clear change in Fe release at station 9 in response to the decline in oxygen (Fig. A.3) in two chambers, measured fluxes based on the first three data points were lower than for the full incubation period. Whether we use the full data set or not does not affect the conclusions of this study.

present in aqueous form (< 0.02 μm) and colloidal/nanoparticulate Fe (0.02 μm–0.2 μm) on average accounted for less than 13% of the total Fe (Fig. 4).

3.5. Suspended matter and sediment Fe composition

The particulate Fe in the suspended matter at six stations as determined with the sequential chemical extraction (Table 2) decreases significantly from the coast to the shelf edge (Fig. 5A, Table A.1). Generally, samples from the lower part of the water column were enriched in Fe when compared to samples taken closer to the water surface. Ferrihydrite and reducible (crystalline) Fe oxides were the dominant reactive Fe phases in the suspended matter at all stations. In general, suspended matter from the lower part of the water column was enriched in ferrihydrite when compared to samples from shallower depths.

The surface sediments at all stations were enriched in easily reducible Fe oxides (Fe_{ox_1}) which includes ferrihydrite (Fig. 6). Fe(II) phases and reducible (crystalline) Fe oxides, with the former mostly consisting of FeS and Fe carbonate, contributed a variable fraction. Magnetite was a minor phase in the sediment. The coastal stations 9 and 13 were characterized by the highest total Fe contents, which range up to ca. 1200 μmol g^{-1}. At all stations, the top sediment layer of 1 to 3 cm was strongly enriched in Fe_{ox_1} and Fe_{ox_2} and total Fe relative to Al, except for station 9 (Fig. A.8). The Fe/Al ratio increases with distance from the shore, with values of ca. 0.5 to 0.8 wt.% wt. % $^{-1}$ at coastal stations and 1.2 to 2 wt.% wt. % $^{-1}$ at the outer shelf stations. Total S

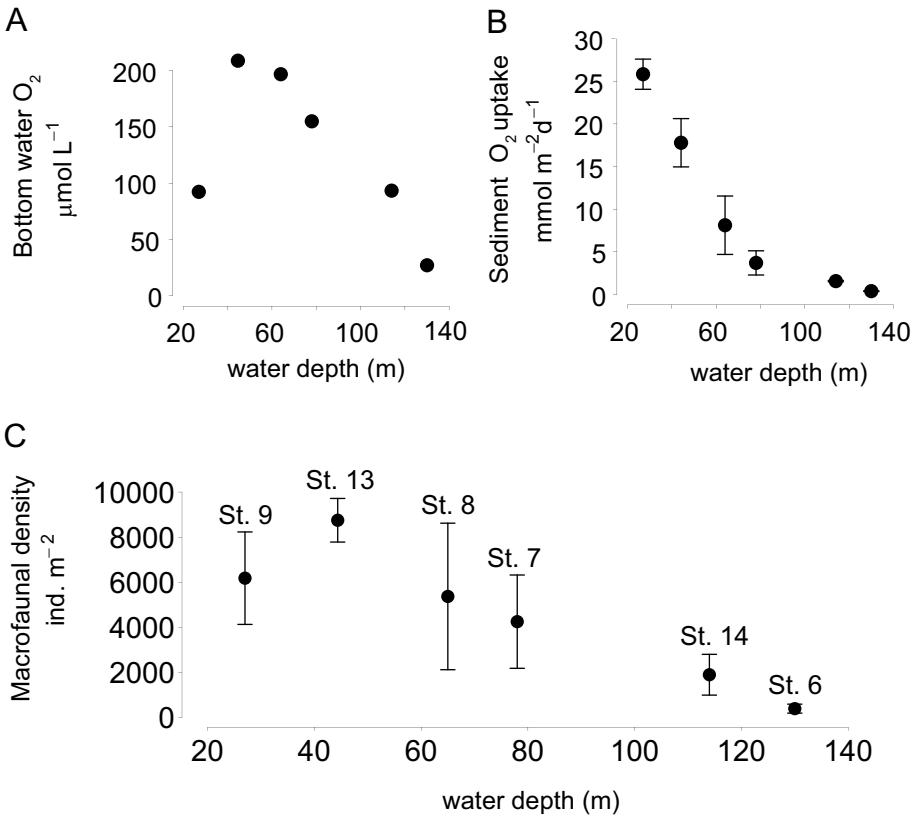

Fig. 2. (A) Bottom water O_2 (in μmol L^{-1}), (B) Sediment O_2 uptake (in mmol m^{-2} d^{-1}; average for 2 or 3 incubation chambers) and (C) Macrofaunal density (individuals per m^2, average and standard deviation for 3 incubation chambers) in the sediment at 6 stations on the northwestern Black Sea shelf (i.e. all stations except 5).

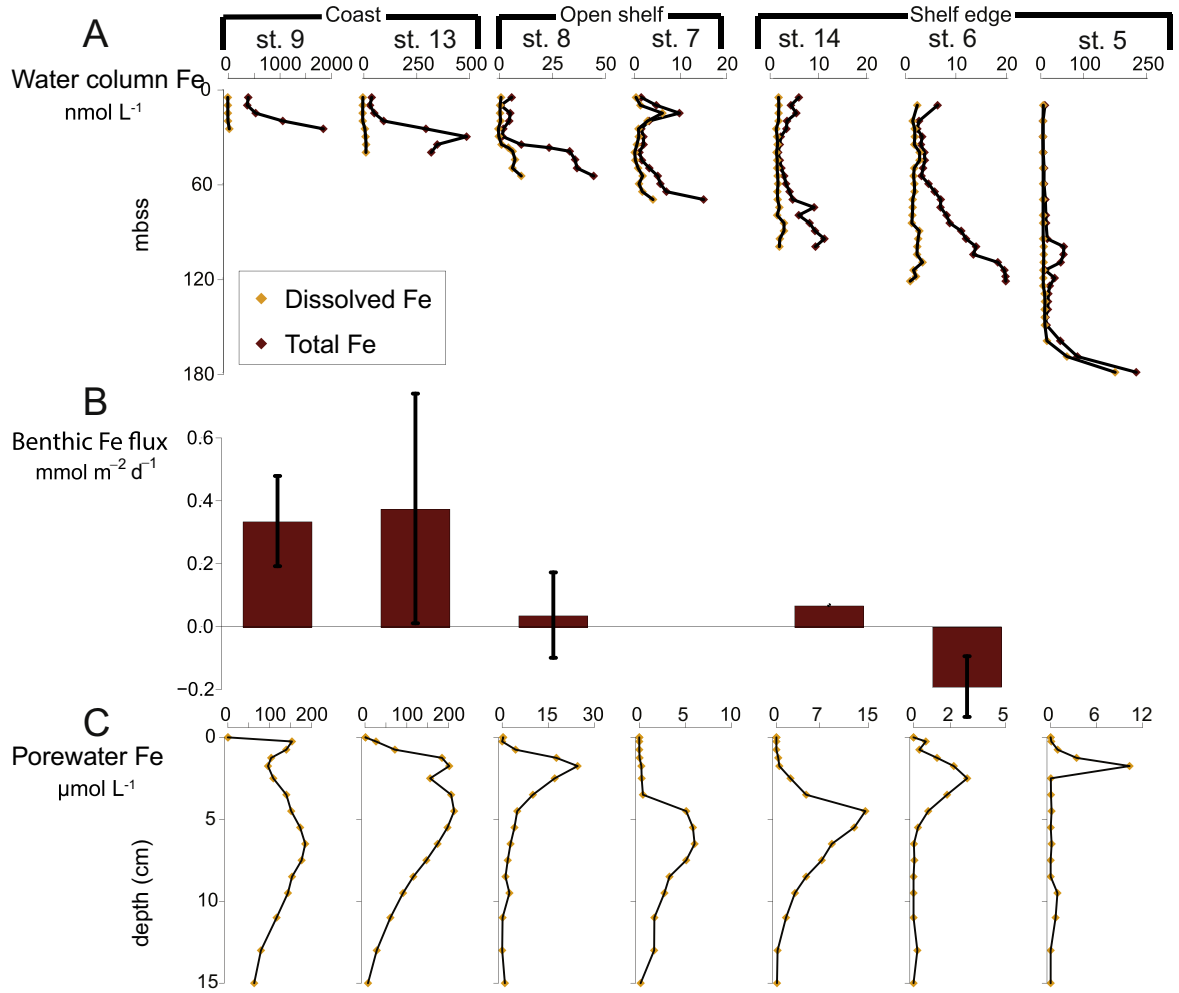

Fig. 3. (A) Water column profiles of total and dissolved Fe (in nM), (B) Benthic Fe fluxes (mmol m^{-2} d^{-1}) and (C) Porewater profiles of Fe (µmol L^{-1}) at our 7 stations on the northwestern Black Sea shelf. Note that no benthic flux measurements are available for station 5 and that a zero flux was observed at station 7.

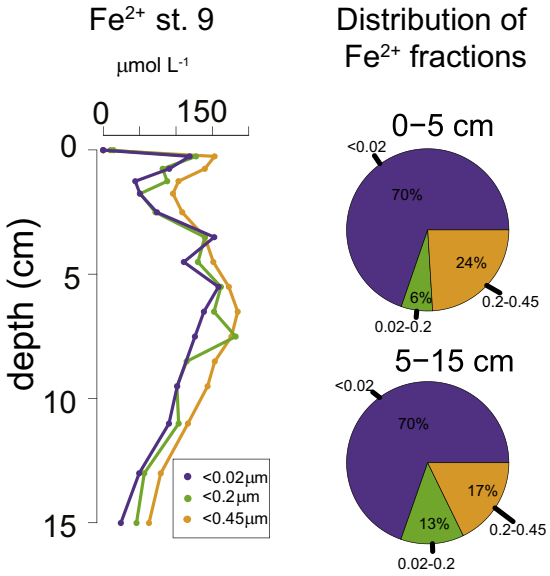

Fig. 4. Porewater depth profiles of filtered fractions of Fe (< 0.02, < 0.2 and < 0.45 µm) at station 9 and average percentages of the different fractions for the depth intervals from 0–5 cm to 5–15 cm.

increases with sediment depth at all stations, with maximum values increasing from the coastal zone towards the shelf edge. Pyrite contents at stations 9, 13 and 8 range from 20 to ~110 µmol g^{-1} and generally increase with depth (Fig. A.9).

3.6. X-ray spectroscopy of suspended matter and sediment

The Fe K-edge XANES and EXAFS spectra for surface sediment and suspended matter show systematic changes that are best explained by variations in the relative content of illite, ferrihydrite and pyrite (Fig. 7A and B). There are especially distinct contrasts between spectra for the coastal station 9, shelf edge station 14 and station 5 in the chemocline. For station 9, a good match between the spectrum for the sediment and illite was found, while for station 14, the spectrum was very similar to that for ferrihydrite. The XANES spectrum for station 5 exhibited a step with a maximum slope around 7118 eV which is characteristic for pyrite and was absent in the spectra of all other stations. The EXAFS spectra support the XANES results. Distinct contrasts between the spectra for stations 9 and 13, for example, can be explained by differences in the abundance of illite and ferrihydrite. The characteristic signatures of crystalline Fe oxides were not observed in the EXAFS spectra. Adding crystalline Fe oxides to the set of endmembers in the linear combination fitting did not lead to significant improvements and illite, ferrihydrite, and pyrite were consistently selected when looking for the best combination of two or three reference spectra. This implies that the content of crystalline Fe oxides in the samples was not

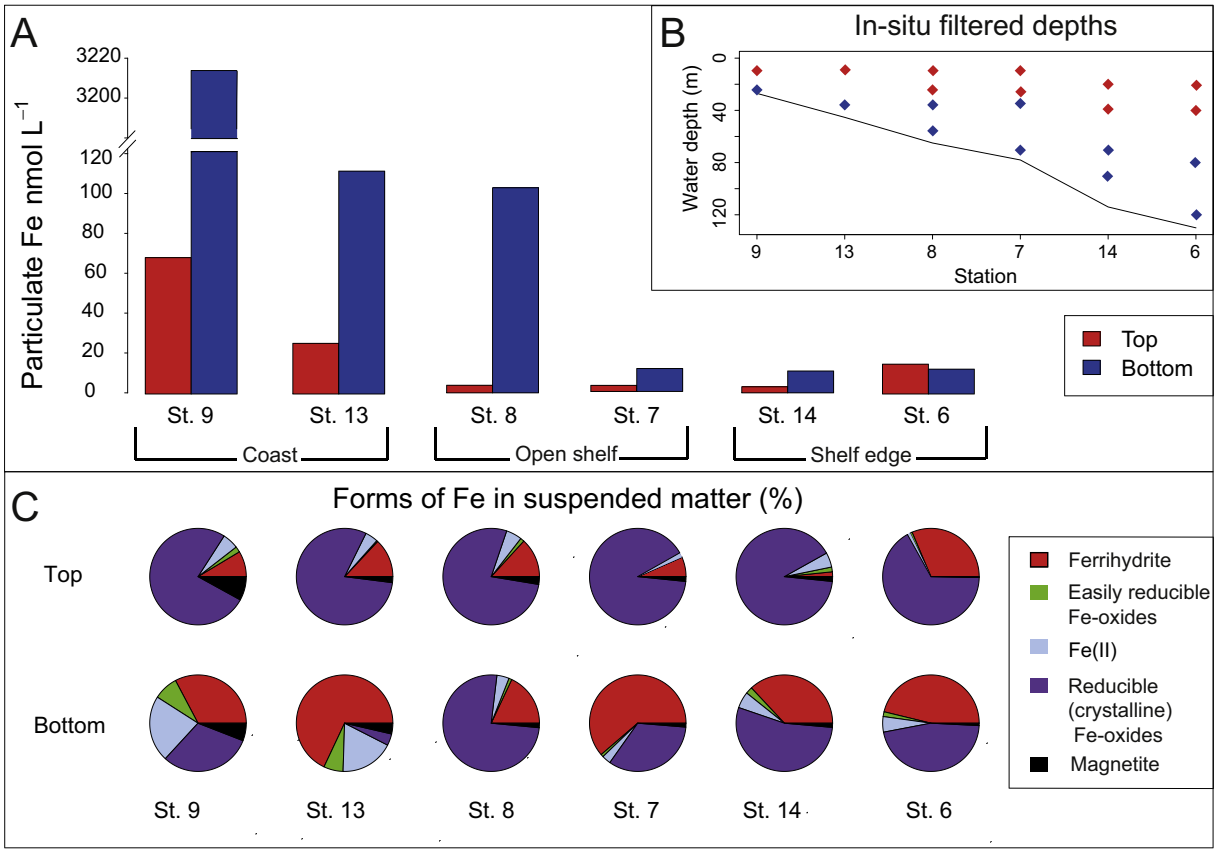

Fig. 5. Fe in suspended matter at 6 stations on the northwestern Black Sea shelf; (A) Particulate Fe refers to the sum of all Fe fractions upon sequential Fe extraction as calculated for the upper (top) and lower (bottom) part of the water column; (B) Water depths at which samples were collected; colors indicate separation into top and bottom. The black line indicates the sediment water interface; (C) Forms of Fe in suspended matter (in %). Data for individual filters are given in Table A.1.

large. At both stations, bulk XAS measurements of the suspended material and surface sediment, were similar indicating a similar Fe mineralogy.

μ-XRF mapping of Fe and K in suspended matter and Fe-XANES spectra at selected spots confirm the presence of clay-Fe at station 9 and both clay-Fe and ferrihydrite at station 13 (Fig. 8 A–C). The ratios of Fe to K fluorescence (expressed in counts, not calibrated) exhibit a lower limit for all investigated areas of the filter from station 13 and area 3 on the filter from station 9 (Fig. 8B). The corresponding baselines are interpreted as the relative intensities of Fe and K fluorescence originating from clay minerals. For station 13, baseline ratios of Fe/K differ between the sub-areas and are roughly around 8, 2, 9 for areas 1, 2 and 3, respectively. Fluorescence intensities of Fe above the baseline are interpreted to indicate the presence of non-silicate Fe. The Fe-XANES spectra (Fig. 8C) collected on various spots at station 13 support the interpretation of the elemental correlations. All spectra at station 13 can be reproduced by linear combination of XANES spectra of illite and ferrihydrite where the contribution of ferrihydrite contributes up to ca. 50% (Fig. 8C). The contribution of ferrihydrite follows the trend in Fe/K ratios: spots that have a Fe/K ratio above the baseline ratio also show higher fractions of ferrihydrite in the linear combination fitting. In contrast, spectra of spots with Fe/K ratios close to the corresponding baseline ratio resemble the spectrum of illite. At station 9, two distinct hotspots for Fe were observed in the μ-XRF map (Area 1 and 2, Fig. 8A). The Fe-XANES spectrum for the spot in area 1 was disturbed and could not be used, but Mn-XANES at the same location pointed towards the presence of spessarite, a Mn-rich garnet (not shown). The Fe-XANES spectra for area 2 show the same features and edge position as biotite (Fig. 8C). The spectra for the background and area 3 resemble those for illite in accordance with the Fe-XANES of the bulk samples (Fig. 7).

Overall, our data indicate a lateral gradient in the forms of Fe in the surface sediment, with the coastal zone stations being dominated by clays, while sediments at the open and outer shelf stations are mostly enriched in ferrihydrite.

4. Discussion

4.1. Organic matter supply drives Fe mobilization in shelf sediments

The Danube river is a major source of terrestrial organic carbon, nutrients and lithogenic particles, including reactive Fe, to the northwestern Black Sea shelf (Popa, 1993; Panin and Jipa, 2002; Poulton and Raiswell, 2002). In the coastal sediments directly in front of the Danube delta, rates of organic matter production, sediment accumulation and benthic mineralization are high, decreasing with distance from the coast (Wijsman et al., 1999). This is confirmed by the offshore decline in NH_4^+ concentrations in the porewater (Fig. A.6). The offshore decline in sediment organic carbon content, O_2 uptake and macrofaunal density observed in our study (Table 3; Fig. 2) is in accordance with these previous observations.

The distinct contrast in depositional conditions near the coast and on the remainder of the shelf has a major impact on porewater Fe concentrations. While porewater Fe reaches values close to 200 μmol L^{-1} in the surface sediments at the coastal stations 9 and 13 (Fig. 3), Fe concentrations were below 30 μmol L^{-1} at the open shelf and shelf edge stations. This implies that only sediments receiving relatively high inputs of organic matter show strong mobilization of Fe in the porewater. At the coastal stations, the abundant presence of organic matter supports a macrofaunal population that transports organic matter and Fe oxides downward into the sediment through mixing. This

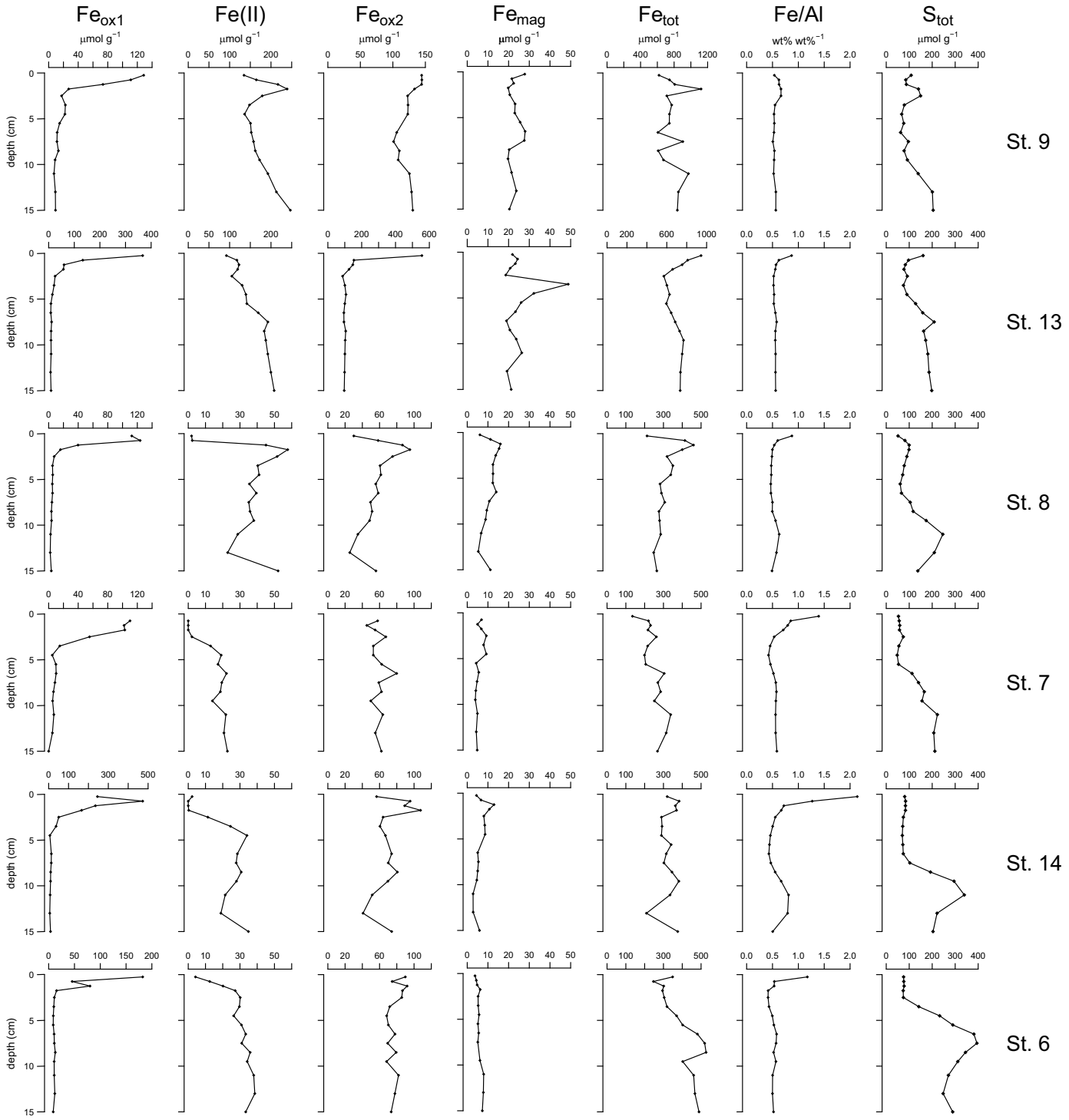

Fig. 6. Solid phase depth profiles of easily reducible Fe oxides (Fe_{ox1}), Fe carbonates and FeS (Fe(II)), reducible (crystalline) Fe oxides (Fe_{ox2}), magnetite (Fe_{mag}), total Fe (Fe_{tot}), Fe/Al and total S (S_{tot}) at six stations on the northwestern Black Sea shelf. Depth profiles of Fe_{ox1}, Fe(II), Fe_{ox2} and Fe_{mag} normalized against Al are plotted in Fig. A.8.

enhances the reductive dissolution of the Fe oxides by promoting dissimilatory Fe reduction and/or sulfate reduction and sulfide-driven Fe reduction (Aller, 1994). At the open shelf and shelf edge stations, in contrast, the organic matter flux is very low and the sediment surface is covered with shells of *Modiolula phaseolina* and *Mytilus galloprovincialis* (Table 4, Wijsman et al., 1999), that do not mix the sediment. In this area, Fe mobilization to the porewater is limited due to relatively low rates of organic matter degradation (Fig. 2; Wijsman et al., 1999).

That bottom water O_2 is not the key control of Fe release is evident from the lack of reductive release of Fe in the porewater at station 6 (Fig. 3). Here, bottom waters are hypoxic (27 µmol L^{-1}) but porewater Fe concentrations remain low (< 3 µmol L^{-1}; Fig. 3C) despite the abundant presence of easily reducible Fe oxides in the surface sediment (ca. 200 µmol g^{-1}; Fig. 6). This emphasizes that mobilization of Fe^{2+} in the sediment and a corresponding benthic Fe flux in hypoxic settings requires a sufficient supply of organic matter. At open shelf and shelf edge regions of the Black Sea, the required organic matter is not consistently present resulting in a limited benthic Fe flux despite a low

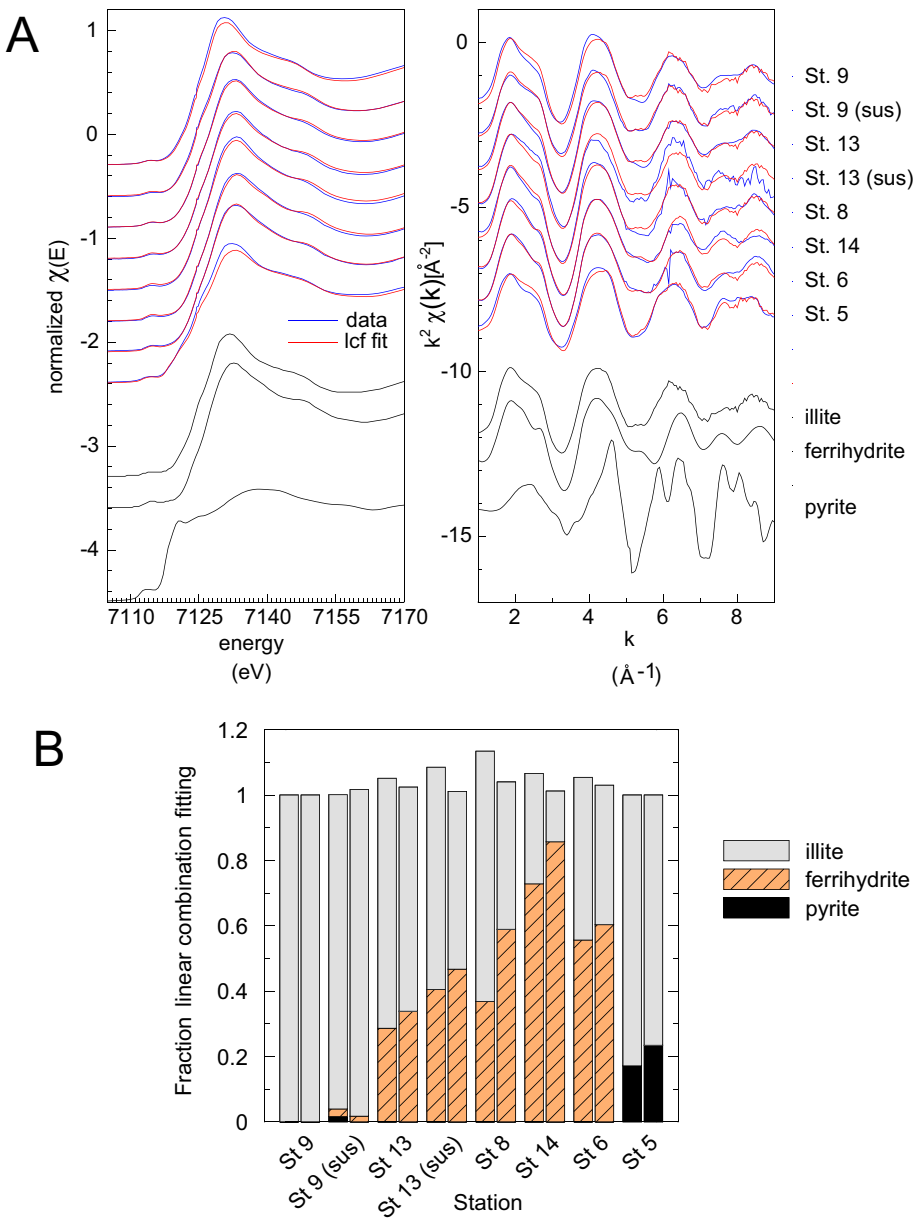

Fig. 7. A. Fe-XANES and EXAFS of powdered surface sediment samples and suspended matter samples from a range of stations compared to the reference materials illite, ferrihydrite and pyrite. B. Relative contribution of the spectra of the reference materials to the EXAFS (left bar) and XANES (right bar) spectra based on linear combination fitting. The uncertainty of the optimized relative contributions varied between 0.03 and 0.08. The sum of the contributions was forced to be 1.0 within in the range of uncertainty. A sum above 1.0 can be, therefore, explained by the cumulative error of the individual contributions and the deviation from 1.0 is not significant.

bottom water O_2 concentration.

At station 9, 70% of the porewater Fe was found to be truly dissolved (< 0.02 μm) with colloidal and/or nanoparticulate Fe accounting for ca. 30%. An important role for truly dissolved Fe was also observed recently for porewaters of shelf sediment in the Celtic Sea (Klar et al., 2017). We hypothesize that the colloidal and/or nanoparticulate Fe at station 9 is formed in sediment burrows.

4.2. Sediment release of Fe: role of diffusion and bioirrigation

The elevated porewater Fe concentrations at the coastal stations 9 and 13 drive the high benthic release of Fe from the sediment to the overlying water (up to on average 0.38 mmol m^{-2} d^{-1}; Fig. 3). Much lower to negligible Fe fluxes are observed at the open shelf and shelf edge stations where porewater Fe concentrations are low. The range in Fe fluxes is of the same order of magnitude as those measured previously in this region with benthic landers (with maxima in dissolved Fe fluxes up to 0.44 and 0.53 mmol m^{-2} d^{-1} Friedl et al., 1998; Friedrich et al., 2002). However, in contrast to Friedrich et al. (2002) we did not find an enhanced benthic flux of Fe near the shelf edge.

Benthic fluxes measured at the coastal stations are, however, rather high when compared to typical fluxes of dissolved Fe reported in sediments overlain by well-oxygenated bottom waters (mostly < 0.05 mmol Fe m^{-2} d^{-1}; Dale et al., 2015). Our values are close to the range of dissolved Fe fluxes reported for river-dominated coastal stations with similar carbon oxidation rates on the Californian continental shelf (up to ~0.3 mmol Fe m^{-2} d^{-1}; Severmann et al., 2010). Bioirrigation was suggested to play an important role in controlling the benthic flux of Fe in these systems.

Quantifying the relative contribution of both diffusion and bioirrigation processes is difficult because of the strong vertical and horizontal variability in porewater chemistry of bioirrigated sediments (Aller, 1980; Aller and Aller, 1998), that is not captured with our sampling methods (e.g. Slomp et al., 1997; Wijsman et al., 2001a; Raiswell and Canfield, 2012; Dale et al., 2015). At the coastal stations, calculated diffusive fluxes are high (i.e. 0.36 –2.23 mmol m^{-2} d^{-1}; Table 5). However, we are likely greatly overestimating the diffusive fluxes at these coastal sites in our calculations because we use a concentration gradient based on the average dissolved Fe concentration in the upper 5 mm of the sediment. We know that the actual gradient will be smaller

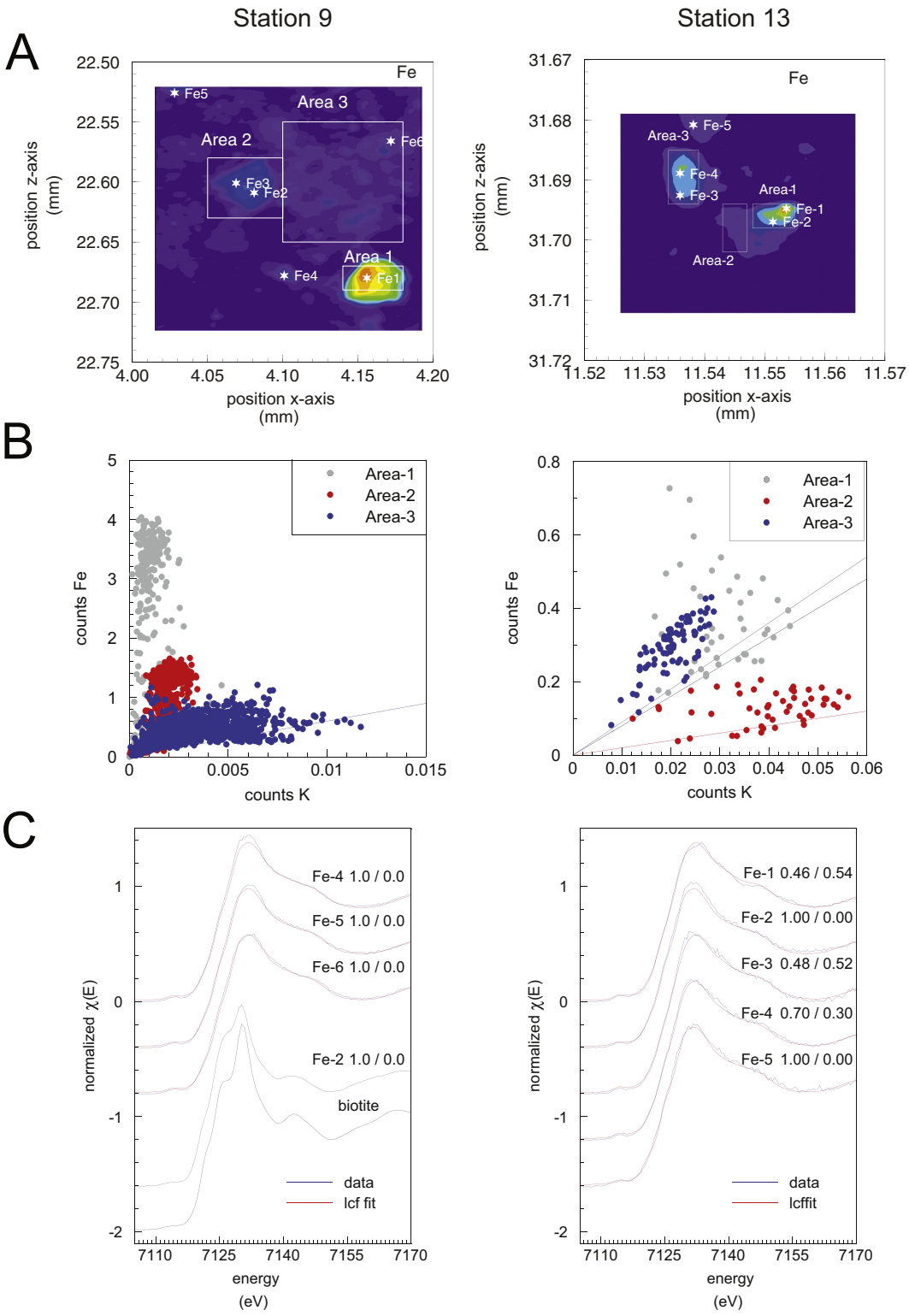

Fig. 8. μ -XRF and Fe-XANES analyses of suspended matter at stations 9 and 13. A. μ-XRF map of Fe. B. Fe and K in μ-XRF maps (fluorescence intensity, counts, not calibrated) in three areas of the sample for each station. The lines are baselines and show the lower limit of the ratio of Fe counts to K counts in the various areas. These baselines reflect the intensity ratio of Fe and K fluorescence of clay minerals in the corresponding area. Higher Fe/K ratios are indicative of enrichments in non-silicate Fe. C. Fe-XANES spectra collected on various spots on the samples; for each spot measurement the fraction of clay-Fe and ferrihydrite in the sample based on linear combination fitting is given. The spectrum for spot Fe-1 is not shown because it was disturbed. The spectrum for spot Fe-3 is not shown because it was similar to that of spot Fe-2.

because of rapid oxidation of Fe^{2+} with O_2 present in the oxic layer (Fig. A.5; Dale et al., 2015). Actual diffusive fluxes are thus expected to be negligible.

With bioirrigation rate determinations, we estimated the potential enhancement of porewater transport by macrofaunal activity with the inert tracer bromide. The corresponding non-local transport coefficients

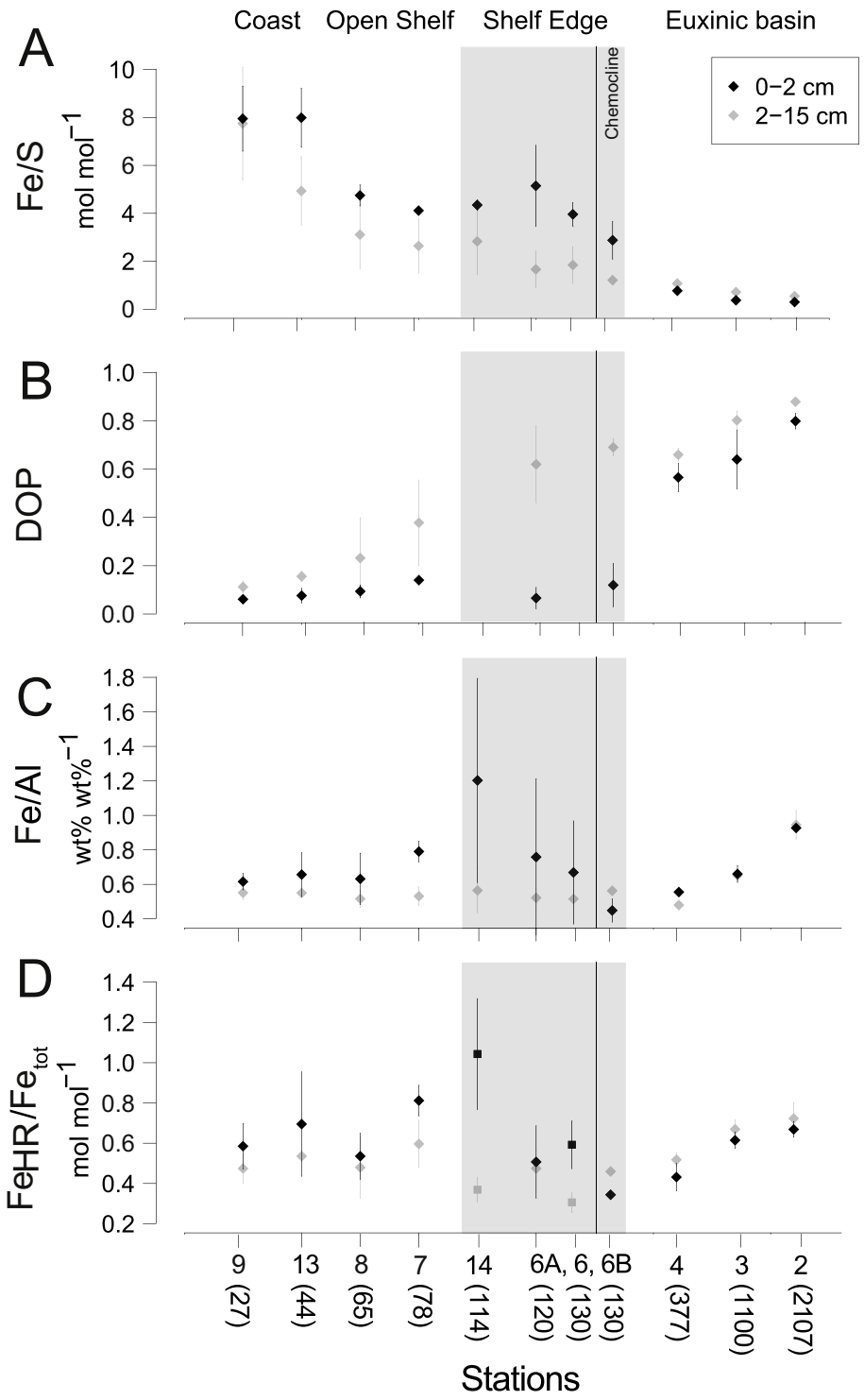

Fig. 9. Indicators for the degree of sulfidization (A, B) and authigenic enrichment of Fe (C, D) in the surface sediment (0–2 cm) and at greater depth (2–15 cm) at 6 of our shelf stations and 5 stations from Kraal et al. (2017) (Table 6). A: Fe_{tot}/S_{tot}; B: degree of pyritization (DOP); C: Fe_{tot}/Al_{tot} and D: Highly reactive Fe/Fe_{tot}. Given that at stations 14 and 6, no FeS_2 data are available, Fe_{HR} is based on fractions (2) to (4) from Table 2 only (indicated as a square instead of a diamond in panel D).

of 0.21 to 0.41 d^{-1} at the coastal stations fall within the high end of the range typically observed in coastal surface sediments (Martin and Banta, 1992; Boudreau, 1998; Schlüter et al., 2000). The potential maximum enhancement of Fe release through bioirrigation can be calculated from these coefficients and the porewater Fe profile, by integrating the following bioirrigation rate (R) term with depth (Eq. (2)),

$$R = \int_0^b \alpha(x)([Fe](x) - [Fe](0) \quad (2)$$

where $\alpha(x)$ stands for the non-local transport coefficient as a function of depth in the sediment, [Fe](x) is the porewater concentration of dissolved Fe as a function of depth, [Fe](0) is the dissolved Fe concentration in the overlying water and b is the maximum depth where bioirrigation takes place (Fig. A.7). At stations 9 and 13, the maximum bioirrigative flux of Fe calculated from this equation is 3.8 and 2.4 mmol m^{-2} d^{-1}, respectively. These potential bioirrigative fluxes of Fe are one order of magnitude higher than the *in-situ* measured Fe

fluxes. This suggest that a major proportion of the Fe is retained in the sediment through formation of Fe oxides in oxygenated burrows (Meile et al., 2005). However, we find that Fe still escapes to the overlying water and suggests that bioirrigation mainly controls this flux of Fe^{2+} and colloidal or nanoparticulate Fe out of macrofaunal burrows.

4.3. Fe shuttling over the Black Sea shelf and into the deep basin

Most Fe in the water column along our water depth transect is present as particulate Fe (> 0.2 μm) (Fig. 3) with concentrations decreasing with increasing distance from the shore. Similar general trends in dissolved and particulate Fe were reported for a range of stations in a nearby area in the summer of 1995 (Tankéré et al., 2001), suggesting that this is a consistent feature of the northwestern Black Sea shelf.

High Fe release from the coastal stations led to elevated concentrations of dissolved Fe in the water column near the sediment water interface at stations 9, 13 and 8 (Figs. 3A and A.10). Given the instability of Fe^{2+} in an oxygenated environment at circumneutral pH, the dissolved Fe in the water column was likely in the form of Fe^{3+} complexed with organic ligands (Wu et al., 2001; Gerringa et al., 2016). The plume of dissolved Fe does not extend beyond station 8 because of limited benthic release of Fe at the open shelf and shelf edge stations. Particulate Fe is enriched in the lower part of the water column at all stations on the shelf, but particularly in the coastal zone (Figs. 3A and A.10), suggesting that benthic Fe release is a key source of Fe to the water column. The results of our sequential extractions suggest that Fe in suspended matter and the surface sediment is present as ferrihydrite and reducible (crystalline) Fe oxides (Figs. 5 and 6). However, while the XAS results confirm a role for ferrihydrite in both the suspended matter and surface sediment (Fig. 7), there is little evidence for a major contribution of reducible (crystalline) Fe oxides. Instead, there is a strong contribution of clay-Fe. We have two possible explanations. First, we may extract Fe from clays in the dithionite solution used in step 3 of our extraction procedure (Fe_{ox_2}; Table 2), which could lead to an overestimation of the Fe_{ox_2}. Second, we may not be accurately separating ferrihydrite and clay-Fe in the XAS analysis if the clay-Fe in the Black Sea differs from our illite standard, which could lead to an uncertainty in the illite fraction. Regardless of the absolute contribution of each phase, both sequential extraction and XAS results suggest the highest concentrations of easily reducible Fe oxides in the surface sediments at the shelf edge.

At the coastal stations, both the porewater and water column profiles suggest that Fe oxides are actively precipitating in the surface sediment and water column (Fig. 3), with the suspended matter at station 13 being particularly enriched in easily reducible Fe oxides (Figs. 5C and 7). The presence of clay-Fe suggests that there is also riverine input of Fe-bearing material, possibly as resuspended surface sediment. At the open shelf and shelf edge stations lateral transfer through repeated deposition and resuspension controls the composition of the particulate Fe in the water column since there is practically no release of Fe from the sediment in this area (Fig. 3B).

Further insight into the dynamics of Fe on the shelf and its ultimate fate can be obtained by combining our data with those of Kraal et al. (2017) to create a water depth transect that extends into the deep basin (Table A.2, Fig. A.11). We focus on four indicators that provide insight into the degree to which Fe is associated with sulfur and the degree to which Fe is authigenically enriched in the surface sediment (0–2 cm) and at depth (2–15 cm) in four regions, namely the coastal zone, open shelf, shelf edge and euxinic basin (Fig. 9).

The first two indicators are the total Fe/S ratio and the degree of pyritization (DOP), with the latter being defined as the fraction of highly reactive Fe (Fe_{HR}) that is bound in pyrite (Berner, 1970; Raiswell et al., 1988). Fe_{HR}, in turn, is defined as the sum of pyrite and all forms of Fe extracted in our sequential extraction procedure for sediments (Table 2). The trends in the Fe/S and DOP reflect increased sulfidization of Fe from the coastal zone to the euxinic basin and with depth in the sediment, (Fig. 9A, B; Table 6), as reported previously Canfield et al. (1996), Wijsman et al. (2001a), Lyons and Severmann (2006). Importantly, the coastal sediments, which act as a source of Fe to the shelf, are characterized by the lowest degree of pyritization (DOP < 0.2) and high Fe/S. Such a low degree of pyritization is typical for rapidly accumulating coastal sediments with high macrofaunal activity where sulfide that is produced is reoxidized and not bound to Fe (Jørgensen, 1977). This provides conditions where Fe can accumulate in the porewater and escape to the overlying water. At the open shelf and shelf edge stations, in contrast, a larger proportion of the Fe is sulfidized (DOP > 0.2), particularly at depth, through long-term exposure of the slowly accumulating sediment to sulfide produced through sulfate reduction (Weber et al., 2001; Slomp et al., 2013). In the euxinic deep basin, DOP values increase towards 1, typical for iron-limited pyrite formation in sulfidic waters where pyritization of Fe_{HR} is nearly complete (Berner, 1984; Raiswell and Berner, 1985).

Table 6
Average values of sediment indicators for degree of sulfidization (Fe/S and DOP) and authigenic enrichments of Fe (Fe/Al and Fe_{HR}/Fe_{tot}) for 4 different areas for depth intervals 0–2 and 2–15 cm in the sediment.

	Area	Fe/S mol mol^{-1}	DOP	Fe/Al wt.% wt.%$^{-1}$	Fe_{HR}/Fe_{tot} mol mol^{-1}
0–2 cm	Coast	7.95	0.07	0.63	0.64
	Open shelf	4.41	0.12	0.71	0.67
	Shelf edge	4.06	0.09	0.77	0.62
	Euxinic basin	0.46	0.67	0.71	0.57
2–15 cm	Coast	6.32	0.13	0.55	0.50
	Open shelf	2.85	0.30	0.52	0.54
	Shelf edge	1.86	0.65	0.54	0.40
	Euxinic basin	0.76	0.78	0.69	0.63

The second two indicators are associated with the degree to which Fe is authigenically enriched, are the ratio of Fe/Al and Fe_{HR}/Fe_{tot}. Both ratios have been used previously to assess the sources and sinks of Fe in sediments of the Black Sea and other basins and are thought to carry the same information although exact definitions of Fe_{HR} vary (Wijsman et al., 2001a; Anderson and Raiswell, 2004; Lyons and Severmann, 2006). Trends in both ratios generally are similar along our water depth transect (Fig. 9C and D). However, there is a striking contrast between the Fe/Al and Fe_{HR}/Fe_{tot} ratios in the upper 2 cm of the sediment and deeper sediment layers. The high ratios in the 0–2 cm layer on the shelf edge (> 1) are in accordance with the abundant presence of ferrihydrite. This strong enrichment of Fe at the sediment-water interface at the shelf edge is likely mainly due to lateral transport of Fe from the coastal zone and open shelf. Upward diffusing Fe^{2+} could also contribute to the surface enrichment of total Fe at the shelf edge. However, given the low upward diffusive Fe^{2+} flux at stations 14 and 6, its contribution is expected to be small (Table A.3). Additionally, transport of Fe from the chemocline to the shelf edge might contribute to the surface enrichment at station 6 (Figs. 3A and A.10). Physical transport of the ferrihydrite likely acts as a key source of Fe for the deep basin in the absence of benthic Fe release at the shelf edge. The classical signature of relatively low Fe/Al (and Fe_{HR}/Fe_{tot}) ratios on the oxic shelf (< 0.6) relative to the deep basin (> 0.6) (Lyons and Severmann, 2006) is visible only in the deeper sediment layers (2–15 cm depth; Table 6). Our results emphasize that the ultimate fate of most of the ferrihydrite in the surface sediment on the shelf is burial in the deep basin.

From our findings, a picture emerges in which diagenetic recycling of Fe in organic-rich, bioturbated and bioirrigated sediments in the coastal zone drives the shuttling of ferrihydrite over the continental shelf (Fig. 10). Input of reactive Fe from the Danube river likely contributes to the high availability of Fe in the sediment at our coastal stations and the corresponding high Fe/S and DOP values. Our results highlight that sediments receiving high inputs of organic matter and reactive Fe that are overlain by oxic bottom waters can act as a major source of Fe to the

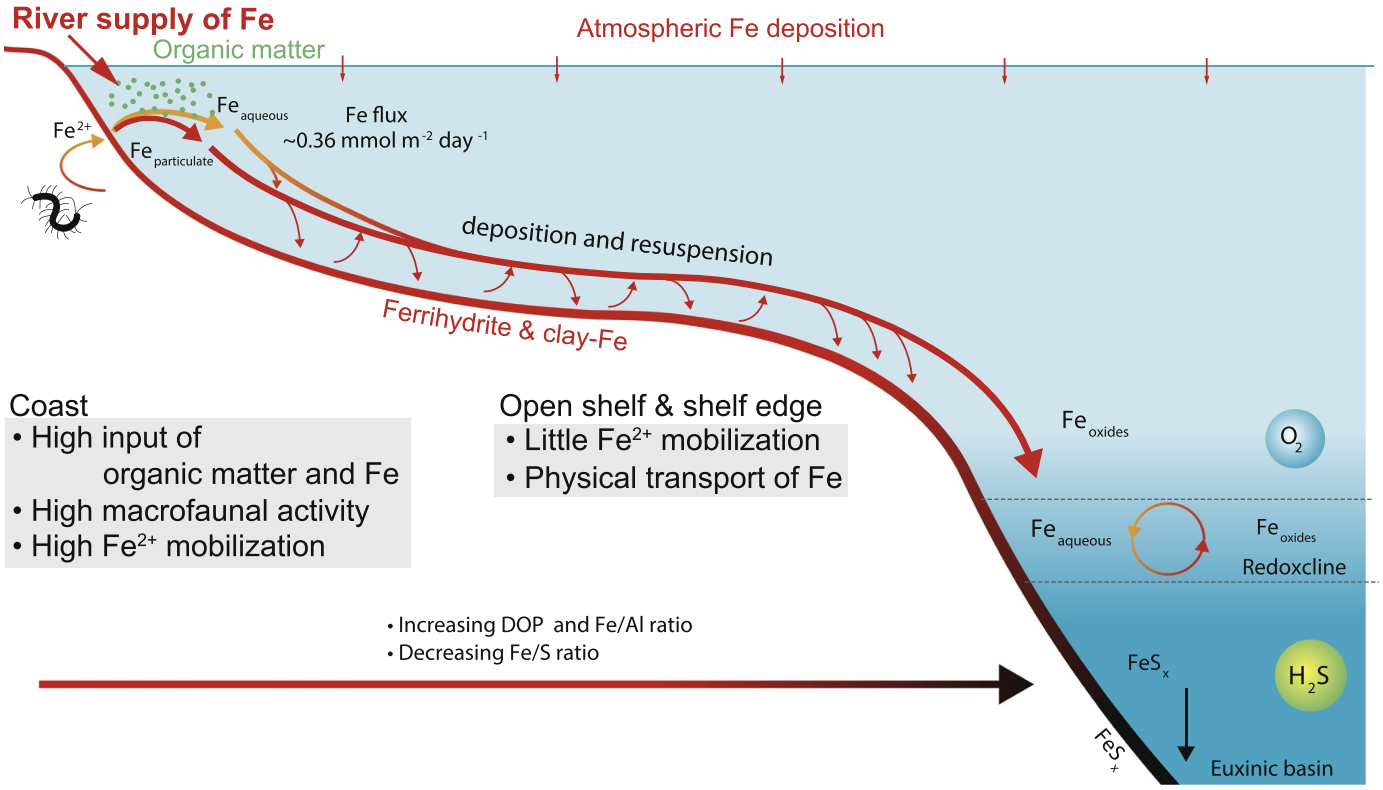

Fig. 10. Schematic overview of Fe-shuttling on the northwestern Black Sea shelf. Red lines and arrows indicate colloidal and particulate Fe (> 0.2 µm), orange arrows indicate dissolved Fe (< 0.2 µm).

water column. This contrasts with conclusions drawn from a diagenetic modeling study for the Black Sea shelf where high rates of organic matter degradation and sulfate reduction were suggested to prevent the release of Fe to porewaters and the overlying water (Wijsman et al., 2001b). However, this is in agreement with the sensitivity analyses presented in Dale et al. (2015) where Fe release could strongly be enhanced at high rates of input of Fe. The lateral transport of Fe in the water column of the open shelf and shelf edge areas is largely controlled by physical transport of particles. At the time of sampling in our study, the waters on the shelf were strongly stratified and the reactive Fe oxides remained in the lower part of the water column. The small enrichment in particulate Fe in the surface water is likely due to atmospheric input of Fe via dust. Winter mixing of the water column might lead to upward transport of particulate Fe to surface waters, as observed in other areas (Vink, 2001; Pollard et al., 2009; Klunder et al., 2011). Our results highlight, however, that oxic shuttling of Fe dominates shelf transport of particulate Fe in the northwestern Black Sea.

4.4. Implications

The coastal zone of the Black Sea is sensitive to human-induced eutrophication and bottom water hypoxia (Bodeanu et al., 1998; Capet et al., 2013). Because biological activity drives the release of Fe from coastal sediments, the immediate effect of a decrease in bioturbation and bioirrigation linked to an expansion of coastal hypoxia (Diaz and Rosenberg, 1995; Levin et al., 2009) could be a lower flux of Fe from the sediment to the overlying water. However, given that the oxidative removal of Fe^{2+} in the surface sediment would also decrease, the net effect would likely be an enhanced efflux of Fe^{2+} from the sediment. Whether this benthic Fe release would be maintained would depend on the balance between the availability of Fe oxides and the production of sulfide in the sediment. This latter response to hypoxia is in accordance with the concept of a redox window for Fe release upon increased hypoxia (Scholz et al., 2014a; Lenz et al., 2015).

Bottom water redox conditions on the open shelf and shelf edge are very sensitive to changes in the position of the Black Sea chemocline. Fluctuations in its position can occur on time scales from seasons to millennia (e.g. Murray et al., 1989; Sinninghe Damsté et al., 1993; Capet et al., 2016) and have been invoked to explain long-term variations in Fe burial in the deep basin (Eckert et al., 2013). During our sampling campaigns in 2013 and 2015, the depth of the chemocline was located at 130 and 150 m depth respectively, which is typical for this region (Arthur and Dean, 1998; Coolen et al., 2009). While the sediments in the redoxcline are depleted in Fe oxides (Stations 6B; Fig. 9C and D), sediments above this water depth zone are highly enriched in Fe oxides (e.g. station 14 and 6; Fig. 6). Changes in the position of the redoxcline could thus lead to mobilization of Fe, if sufficient organic matter is available. Evidence for release of Fe is provided by the low Fe/Al and especially the low Fe_{HR}/Fe_{tot} ratios in the redoxcline (Fig. 9C and D; Table 6). Given the limited input of organic matter in this area and low rates of sulfate reduction (Weber et al., 2001), the release of Fe upon a change in the position of the redoxcline is not necessarily immediate.

Our data suggest that variations in Fe input to the coastal zone could also act as a key control on Fe shuttling on continental shelves. In our study, the sediments with the highest benthic release of Fe are very enriched in Fe relative to S (Fig. 9A, B). While this may be partly explained by efficient reoxidation of sulfide from sulfate reduction linked to bioturbation and bioirrigation (e.g. Jørgensen, 1977), the riverine input of Fe oxides likely also plays a role. A similar explanation was invoked to explain high benthic Fe fluxes in the Eel river area on the California margin (Severmann et al., 2010). These findings suggest that changes in river fluxes of Fe could modulate the strength of the oxic Fe shuttle on continental shelves, by altering the extent of Fe mobilization in the coastal zone. Current functions to predict benthic Fe fluxes based on organic matter inputs and/or bottom water O_2 concentrations alone (Elrod et al., 2004; Dale et al., 2015) thus need to be expanded to include Fe input (as also recognized by Dale et al., 2015) and to include bioirrigation when describing benthic Fe fluxes from bioirrigated

continental shelf sediments in river-dominated areas. Further insight in the release and lateral transport of Fe from such systems is needed for a truly quantitative understanding of Fe transport from continental shelves to the ocean.

5. Conclusions

Our study reveals large benthic fluxes of Fe (~ 0.36 mmol m^{-2} d^{-1}) from organic-rich, coastal sediments overlain by oxic bottom waters on the northwestern Black Sea. We suggest that high rates of bioirrigation drive this benthic release of Fe to the water column. Despite the abundant presence of Fe oxides in surface sediments on the open shelf and at the shelf edge, reductive dissolution of Fe oxides and benthic Fe release is low in these areas because of a limited input of organic matter. This lack of benthic release of Fe is also observed at shelf edge sites where bottom waters are hypoxic. The benthic Fe release in the coastal zone is suggested to act as the key source of the particulate Fe observed in the lower part of the water column over the shelf. We show that this particulate Fe consists of a mixture of both easily reducible Fe oxides (ferrihydrite) and iron associated with clay. The similarity in the composition of the suspended matter and the surface sediment suggests that transport of Fe towards the shelf edge mainly takes place through deposition and resuspension of particles. We find no evidence for repeated oxidation and reduction of Fe during this lateral transport, emphasizing the role of physical transport processes for Fe shuttling. Coastal sediments are characterized by relatively low Fe/Al ratios compared to those for the open shelf and shelf edge supporting the role of the coastal zone as a source of Fe. Besides variations in coastal hypoxia and the position of the chemocline on the shelf and slope, changes in the availability of organic matter and reactive Fe linked to river input at coastal sites likely contribute to temporal variations in Fe shuttling on the Black Sea shelf.

Acknowledgments

We thank the captain, crew and technicians and Amy Kuzminov aboard *R/V* Pelagia in September 2015 for their assistance and D. van de Meent, T. Claessen, T. Zalm, A. van Dijk and R.K. Groeneveld for their analytical assistance in Utrecht. This research was funded by NWO-Vici grant 865.13.005 (to CPS). PK acknowledges support from NWO-Veni grant 863.14.014. We further thank the staff of the DUBBLE beamline (BM 26a) at the European Synchrotron Radiation Facility (ESRF) and of beamline ID21 and local contacts D. Banerjee, W. de Nolf and A.E. Pradas del Real. Funding at the DUBBLE beamline was granted by the Netherlands Organisation for Scientific Research (NWO experiment 26-01-1094) and by the ESRF (ES 591 (ID-21)).

Appendix A. Appendices

A.1. Bioirrigation model

Porewater bromide is modeled using a 1-D, nonlocal exchange function (Emerson et al., 1984; Boudreau, 1984). Here, dissolved bromide is described as (Eq. (4)),

$$\frac{\partial(\varphi c)}{\partial t} = \frac{\partial}{\partial z}\left(\varphi D_s \frac{\partial c}{\partial z}\right) - \varphi\alpha(c - c_0) \tag{4}$$

where φ is the depth dependent sediment porosity (Fig. A.12), z is depth in the sediment (cm) and D_s is the sediment diffusion coefficient for bromide. The molecular diffusion coefficients D_s at stations 9 and 13 were corrected for tortuosity in the porous medium (Boudreau, 1996) and for the ambient salinity S, temperature T (Table 3) and P, 2.73 and 3.94 bar respectively, using the R package CRAN: marelac (Soetaert et al., 2010), which implements the constitutive relations listed in (Boudreau, 1997). α is the nonlocal bioirrigation function for bromide, which is assumed to be time-invariant. c is the concentration of bromide in the porewater and c_0 is the bromide concentration of the overlying water.

In the model, porosity is interpolated linearly for every depth layer in the model (1 layer every mm) between measured points. The bioirrigation function (α) was determined by fitting porewater bromide depth profiles after incubation to Eq. (4).

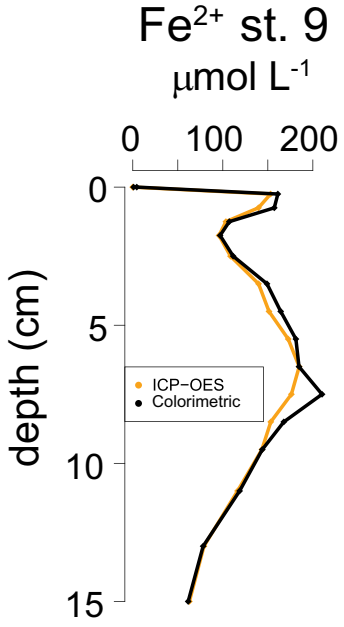

Fig. A.1. Porewater depth profiles of Fe^{2+} filtered through 0.45 µm at station 9, determined by ICP-OES and colorimetrically.

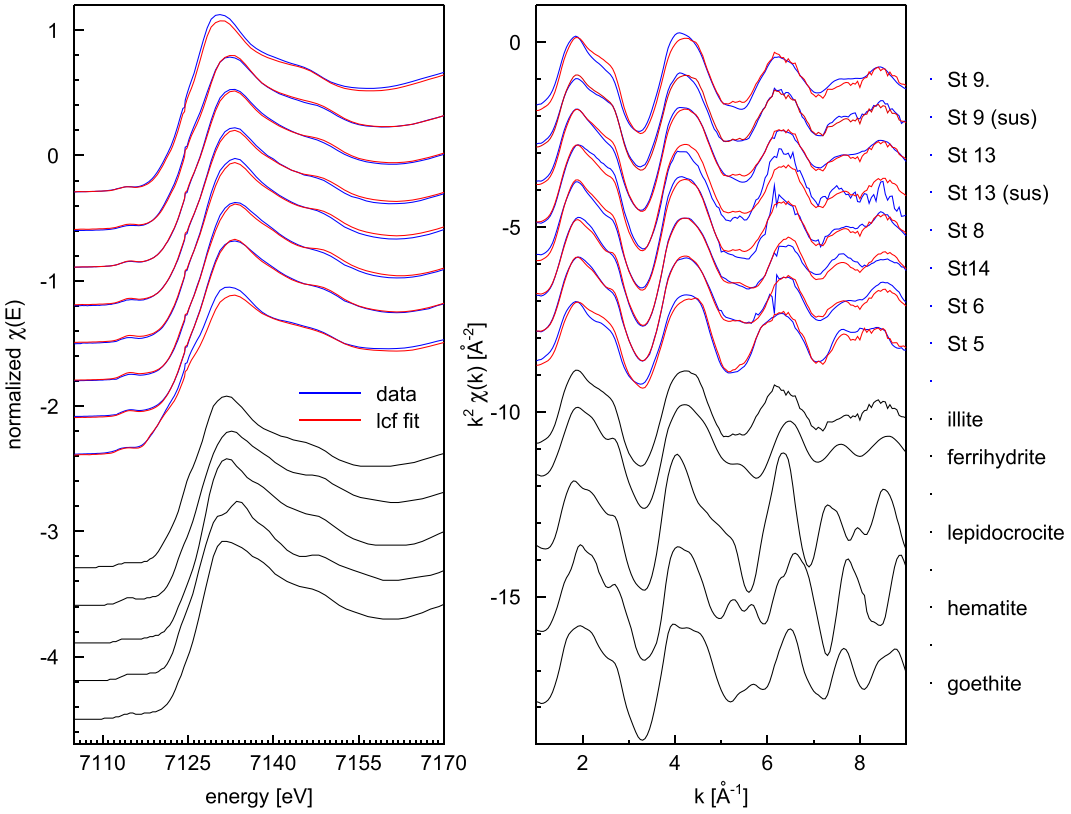

Fig. A.2. Fe-XANES and EXAFS spectra of powdered surface sediment samples and suspended matter samples from a range of stations compared to the reference materials illite, ferrihydrite, lepidocrocite, hematite and geothite.

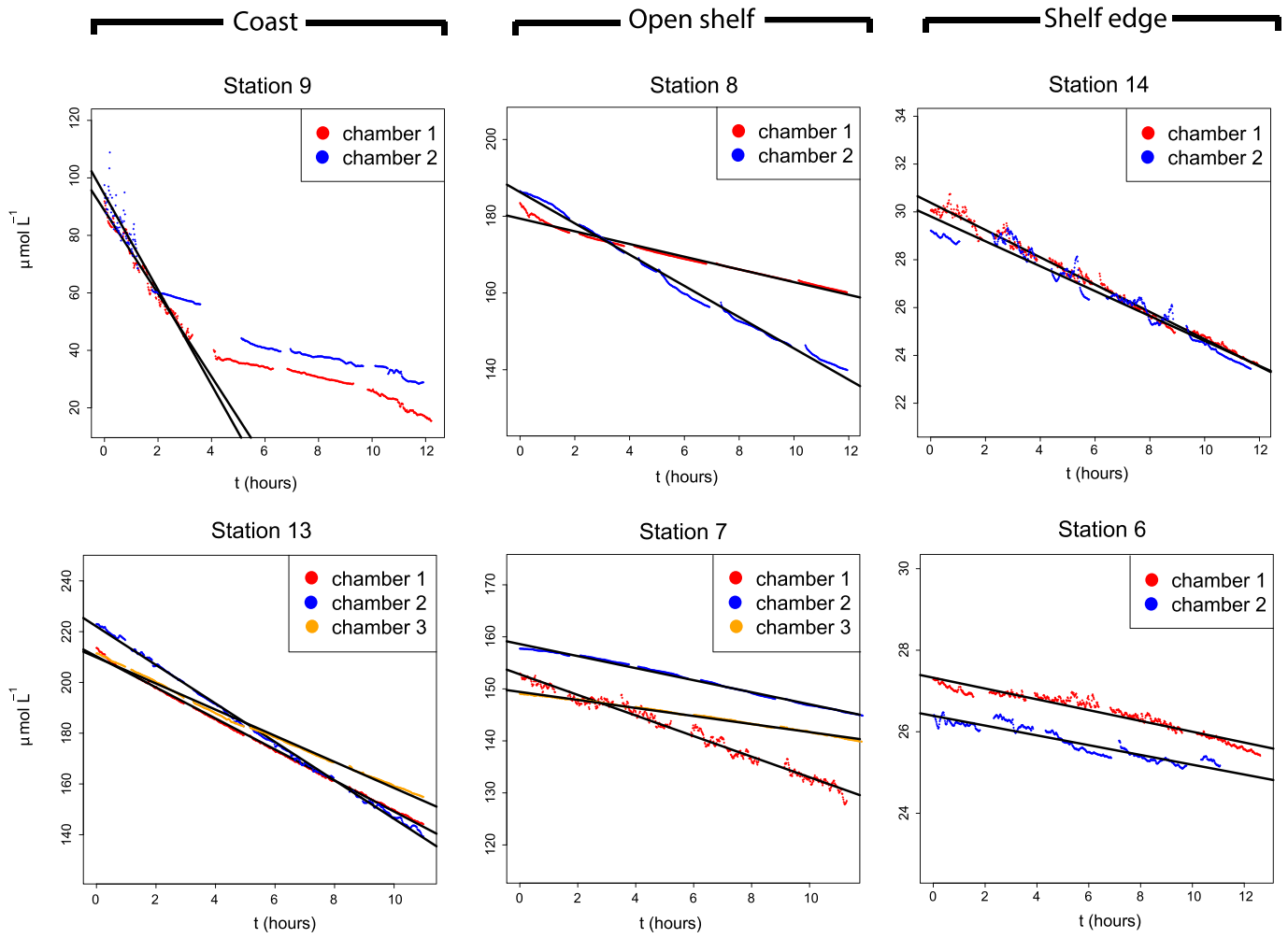

Fig. A.3. Oxygen concentrations in chambers of the benthic lander as determined at six stations. Periods without measurements represent time intervals where optode O_2 measurements were influenced by sample collection and were therefore discarded. Black lines indicate regression lines used to calculate O_2 consumption.

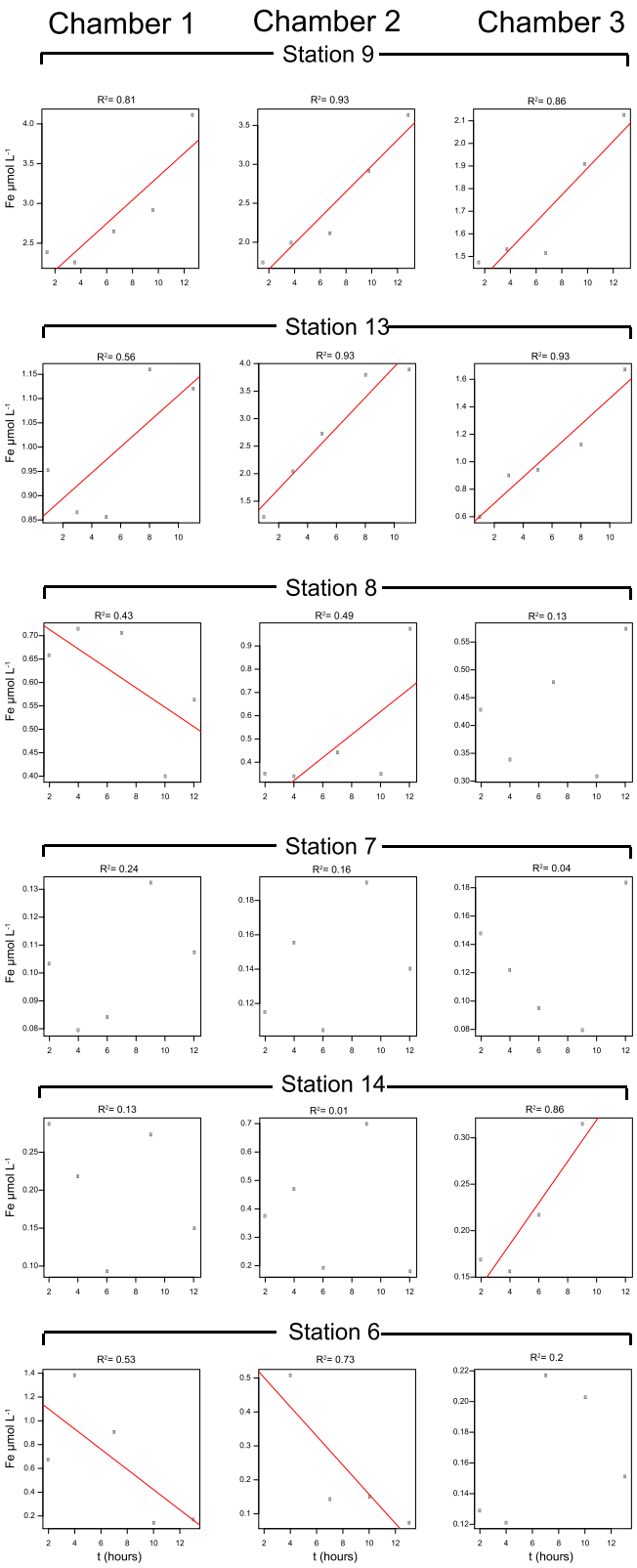

Fig. A.4. Total Fe concentration in benthic lander chambers versus time. Fluxes were calculated using linear regression (red line). Only regressions with $R^2 > 0.3$ were considered following Friedrich et al. (2002).

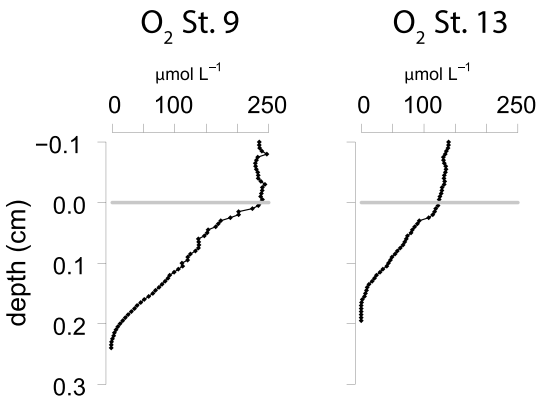

Fig. A.5. Porewater depth profiles of O_2 at stations 9 and 13 determined using micro-electrodes. Gray line indicates the sediment water interface.

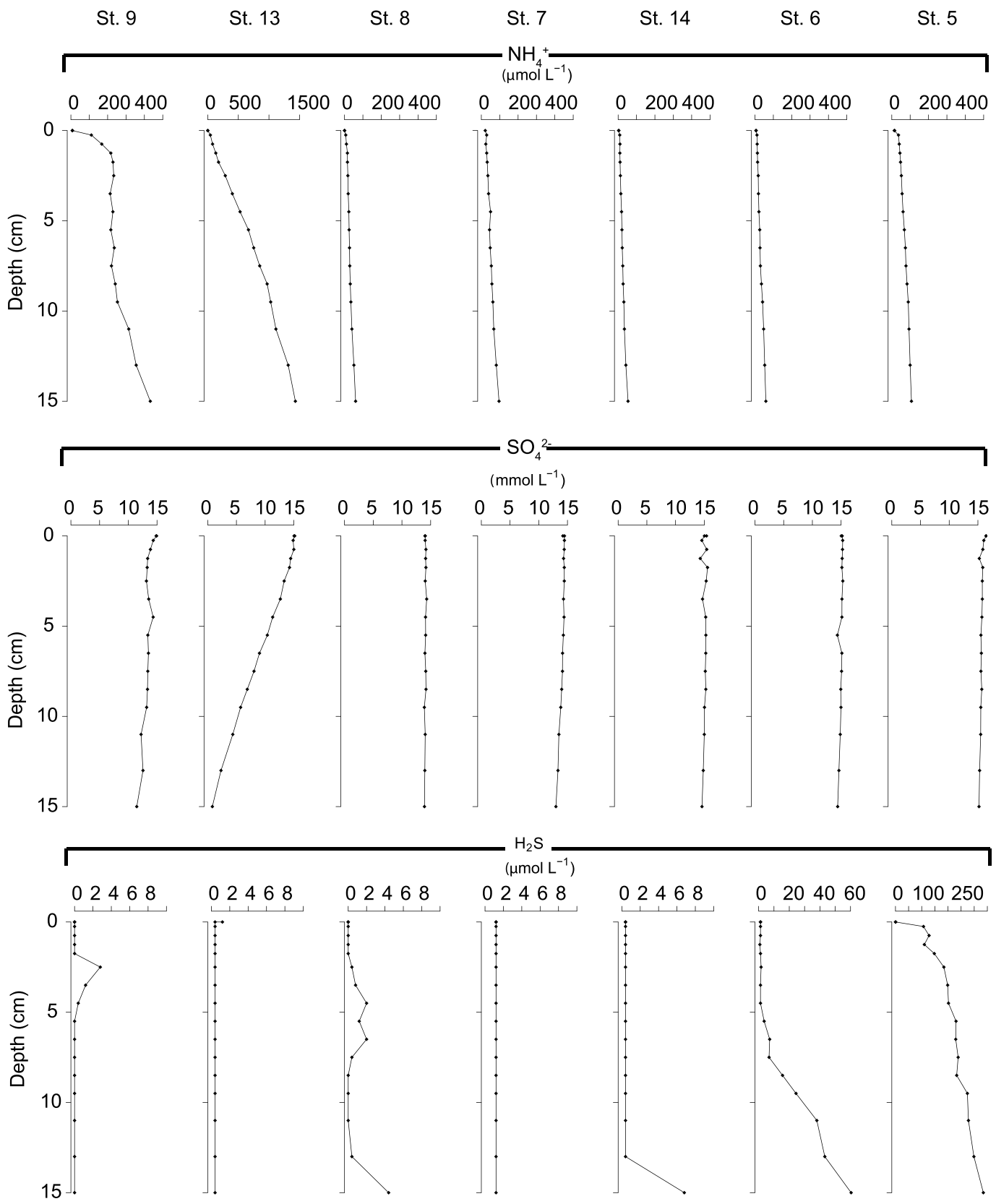

Fig. A.6. Porewater depth profiles of NH_4^+, SO_4^{2-} and H_2S at stations 9, 13, 8, 7, 14, 6 and 5.

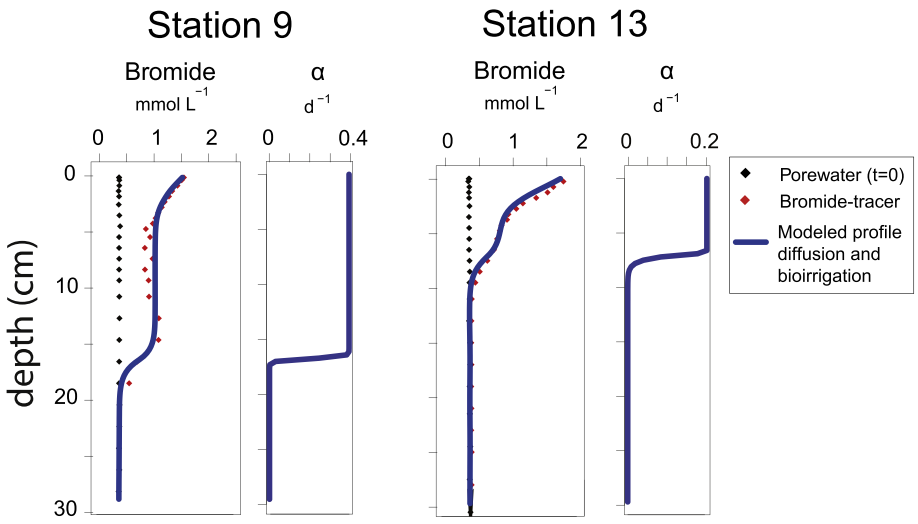

Fig. A.7. Results of bromide tracer incubations at coastal stations 9 and 13. Black diamonds indicate porewater bromide concentrations prior to incubation (t = 0), red diamonds indicate porewater bromide concentrations after incubation. Blue lines indicate modeled porewater bromide concentrations, with bioirrigation.

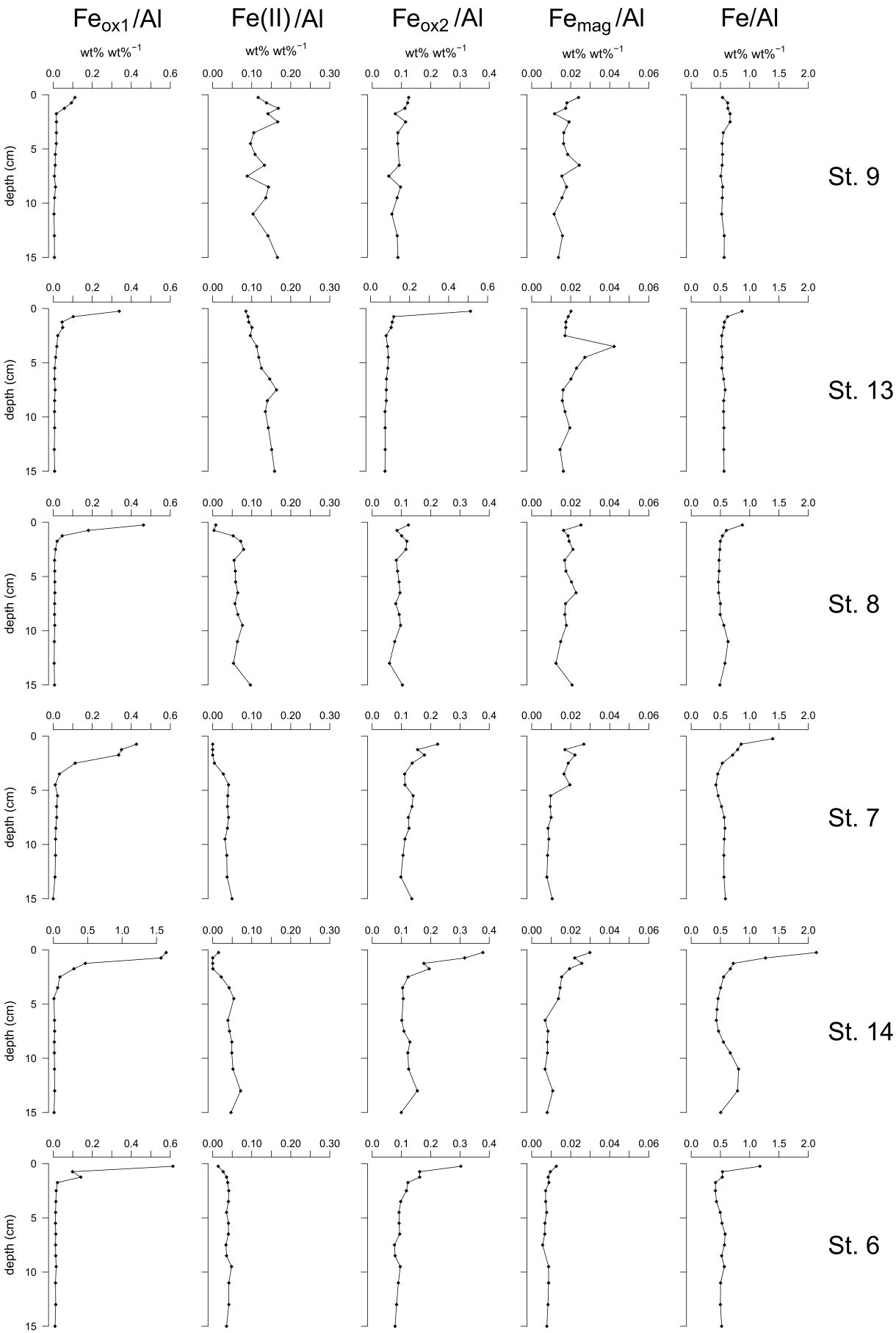

Fig. A.8. Solid phase depth profiles of easily reducible Fe oxides (Fe_{ox1}), Fe carbonates and FeS (Fe(II)), reducible (crystalline) Fe oxides (Fe_{ox2}), magnetite (Fe_{mag}), total Fe (Fe_{tot}) normalized against Al at six stations on the northwestern Black Sea shelf.

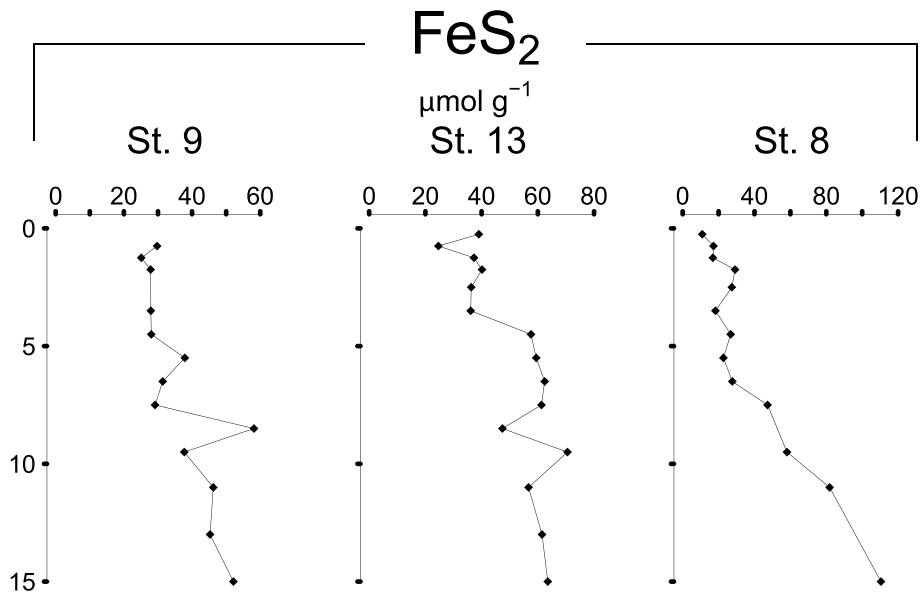

Fig. A.9. Solid phase depth profiles of FeS_2 at stations 9, 13 and 8.

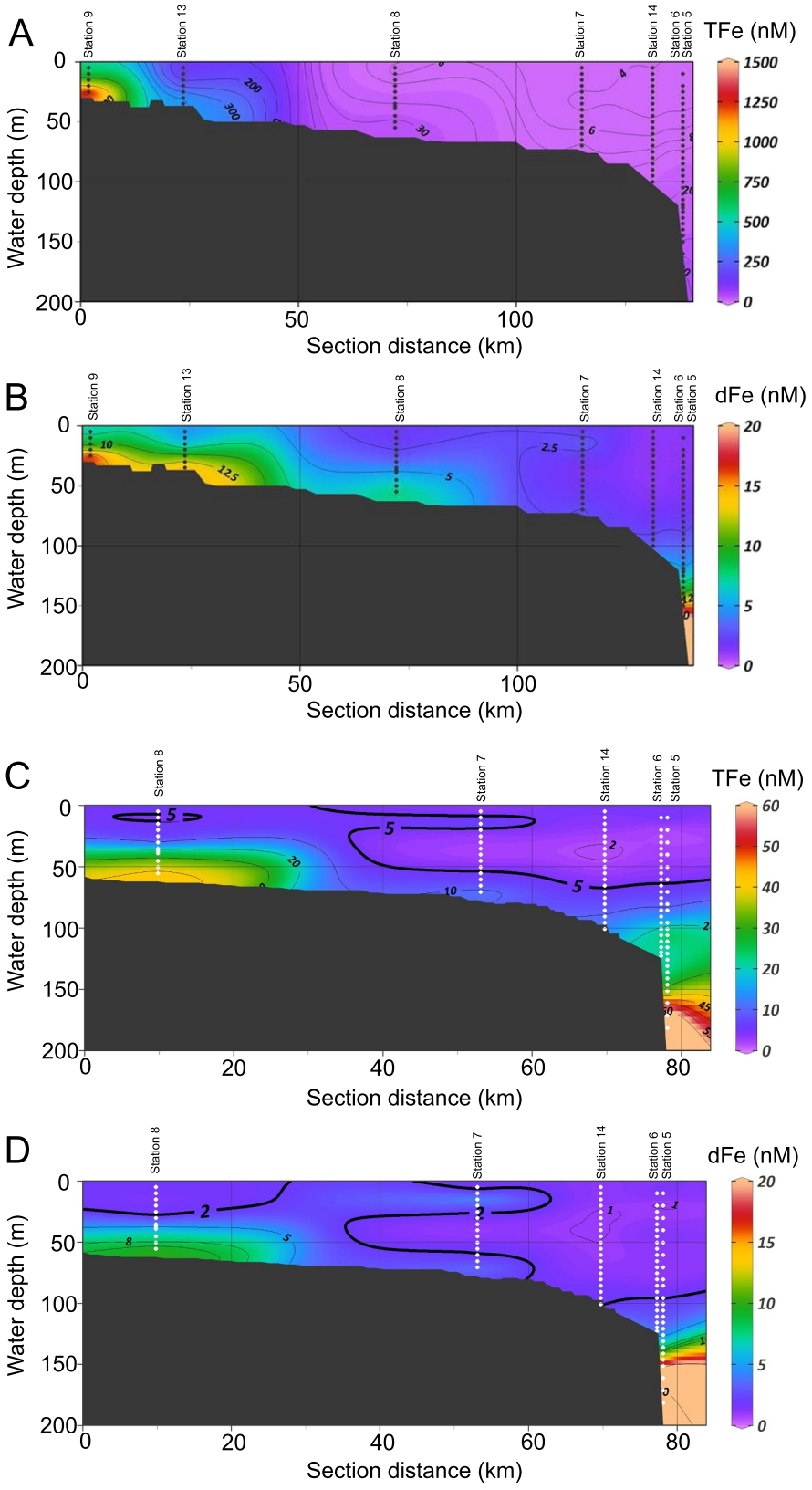

Fig. A.10. Interpolated concentrations of total and dissolved Fe in the water column. A: total Fe for stations 9, 13, 8, 7, 14, 6 and 5; B: dissolved Fe for stations 9, 13, 8, 7, 14, 6 and 5; C: total Fe for stations 8, 7, 14, 6 and 5; D: dissolved Fe for stations 8, 7, 14, 6 and 5. Figure drawn using Ocean Data View (Schlitzer, 2015).

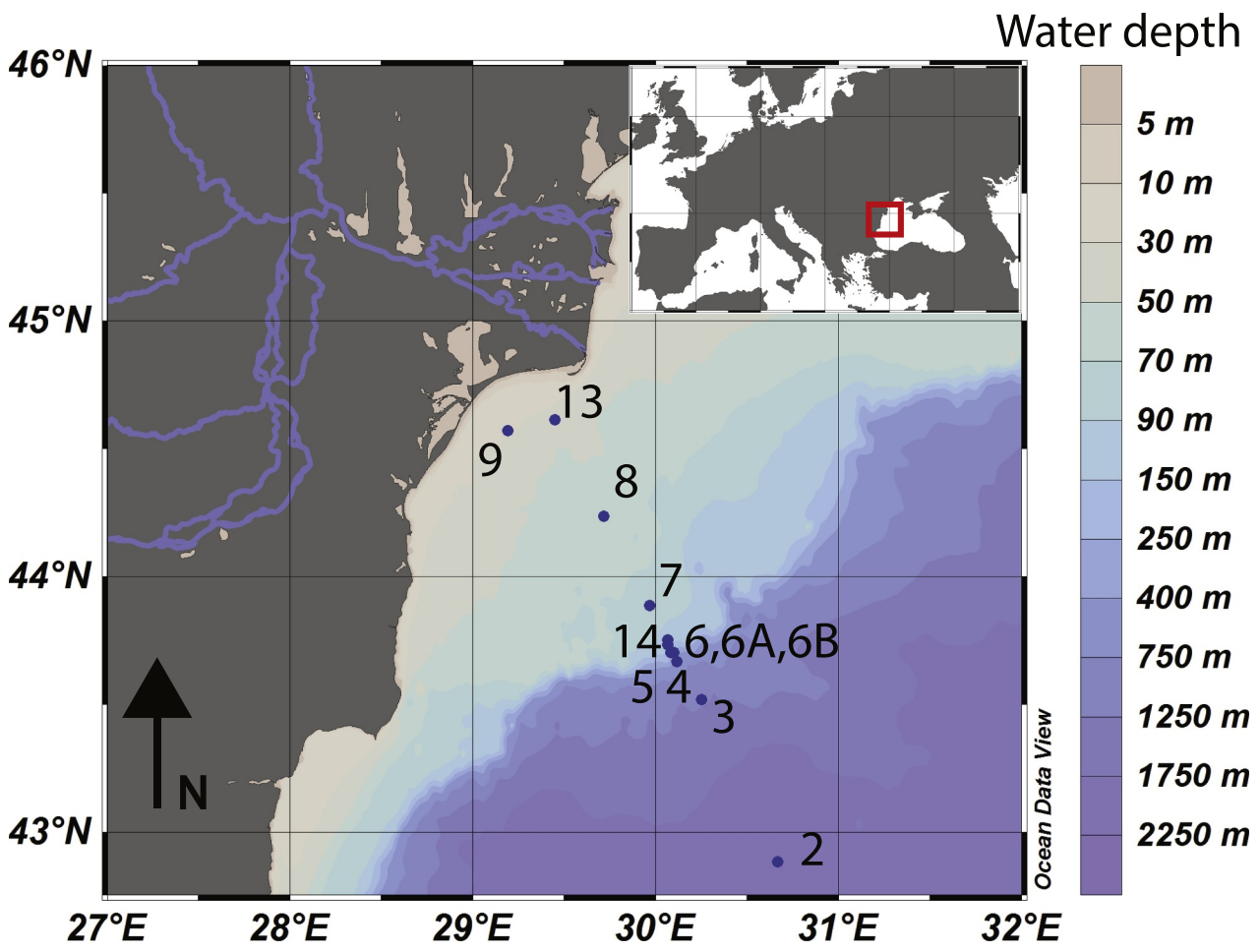

Fig. A.11. Locations of the eleven stations sampled on the northwestern Black Sea shelf and deep basin during two fieldwork campaigns, June 2013 and September 2015 (Table A.2). Figure drawn using Ocean Data View (Schlitzer, 2015).

Fig. A.12. Depth profiles of porosity at stations 9, 13, 8, 7, 14 and 6.

Table A.1
Speciation of Fe for suspended matter collected through *in-situ* filtration at stations 9, 13, 8, 7, 14 and 6. Asc. Fe is ascorbate acid extractable Fe, Fe(II) (Fe carbonate and FeS), Fe_{ox1} easily reducible Fe oxides, Fe_{ox2} reducible (crystalline) Fe oxides and Fe_{mag} magnetite (Table 2).

Station	Depth m	Volume filtered L	Asc. Fe nmol L^{-1}	Fe(II) nmol L^{-1}	Fe_{ox1} nmol L^{-1}	Fe_{ox2} nmol L^{-1}	Magnetite nmol L^{-1}
9	10	36	5.9	3.7	1.3	52	5.5
	25	25	1052.1	714.9	264.6	994.5	191.3
13	10	78	3.3	1.1	0.1	20.4	0.5
	39	91	76	20.1	7.3	4.4	4
8	10	126	1	0.2	0.1	1.8	0
	25	42	0	0.2	0	4.1	0.2
	35	8	10.2	4.6	0.7	146	2
	55	183	26.9	3.9	1.4	9.1	1
7	10	220	0	0.1	0	4.6	0
	25	579	0.4	0	0	0.9	0.1
	35	328	9.5	0	0	2.4	0.1
	70	243	4.6	0.7	0.2	5.3	0.2
14	20	300	0	0.2	0.1	5.5	0.1
	40	579	0.1	0.1	0	0	0
	70	328	4.1	0.5	0.3	6.5	0.1
	90	243	4	0.7	0.2	5.3	0.2
6	20	120	8.6	0.1	0.2	14.5	0.1
	40	273	0.8	0.2	0	5.4	0
	80	379	1.4	0.4	0.1	0	0.1
	120	216	10.1	0.9	0.3	11.5	0.1

Table A.2
Coordinates, water depth, bottom water temperature and salinity at the 12 stations sampled on the northwestern Black Sea shelf. Unit mbss is meters below sea surface. n.a.: not available.

Station	Latitude N	Longitude E	Depth mbss	Temperature °C	BW H_2S μ mol L^{-1}	Year	FeS_2[a] extraction
9	44°34.9′	29°11.4′	27	13.3	0	2015	CRS
13	44°36.5′	29°27.4′	44	9.2	0	2015	CRS
8	44°14.7′	29°43.4′	65	8.2	0	2015	CRS
7	43°53.8′	29°58.6′	78	8.5	0	2013/2015	HNO_3
14	43°45.9′	29°11.3′	114	8.4	0	2015	n.a.
6A	43°44.1′	30°04.4′	120	8.5	0	2013	HNO_3
6	43°42.8′	30°05.1′	130	8.5	0	2015	n.a.
6B	43°42.8′	30°05.1′	130	8.5	0	2013	HNO_3
5	43°42.6′	30°06.1′	180	8.6	0	2015	HNO_3
4	43°40.6′	30°07.5′	377	8.8	8.1	2013	HNO_3
3	43°31.8′	30°15.5′	1100	9	381	2013	HNO_3
2	42°4.8′	29°40.7′	2107	9.1	418	2013	HNO_3

[a] Method used to extract FeS_2 from sediment samples as described in Table 2. For station 7, the FeS_2 extraction was performed on sediment samples collected in 2013.

Table A.3
Calculated contribution of upward diffusing Fe^{2+} to the observed enrichment of total Fe at the sediment-water interface (0–0.5 cm).

Station	Upward diffusing porewater flux mmol m^{-2} yr^{-1}	Calculated surface enrichment μmol g^{-1}	Surface enrichment of total Fe μmol g^{-1}	Contribution of porewater Fe %
14	5.5	20.8	383.3	5.4
6	1.53	5.8	365	1.5

Upward diffusing porewater flux (mmol m^{-2} yr^{-1}) was calculated using Eq. (1). The porewater gradient between 1.75–4.5 cm and 0.75–2.5 cm was taken at stations 14 and 6, respectively. The average porosity over these depth intervals was applied (i.e. 0.87 for both stations; Fig. A.12). The calculated enrichment is based on the upward diffusing flux and the sedimentation rate at the sediment-water interface. At decreasing sedimentation rates, the role of upward diffusion of Fe^{2+} increases. Rates of sediment deposition at the shelf edge stations are low (Friedrich et al., 2002). The sedimentation rate at the open shelf is assumed to be 0.1 cm yr^{-1} (Wijsman et al., 2002). For this calculation we assumed an even lower rate of sedimentation of 0.01 cm yr^{-1}. The sediment enrichment (μmol g^{-1}) was calculated as follows,

Sed. enrichment = upward diffusing flux/(sedimentation rate * sediment density *10^4) (3)

The upward diffusing flux is expressed in units of μmol m^{-2} yr^{-1} and sedimentation rate in cm yr^{-1}. Sediment density was assumed to be 2.65 g cm^{-3} (Burdige, 2006). The contribution of the porewater flux is the percentage of the calculated surface enrichment based on upward diffusing Fe^{2+} divided by the surface concentration of total Fe at 0–0.5 cm depth.

Appendix B. Supplementary data

Supplementary data to this article can be found online at https://doi.org/10.1016/j.chemgeo.2018.10.024.

References

Aller, R.C., 1980. Diagenetic processes near the sediment-water interface of Long Island Sound. II. Fe and Mn. Adv. Geophys. 22, 351–415. https://doi.org/10.1016/S0065-2687(08)60068-0.

Aller, R.C., 1982. The effects of macrobenthos on chemical properties of marine sediment and overlying water. Animal-Sediment Relations. pp. 53–102. https://doi.org/10.1007/978-1-4757-1317-62.

Aller, R.C., 1994. Bioturbation and remineralization of sedimentary organic matter: effects of redox oscillation. Chem. Geol. 114 (3-4), 331–345. https://doi.org/10.1016/0009-2541(94)90062-0.

Aller, R.C., Aller, J.Y., 1998. The effect of biogenic irrigation intensity and solute exchange on diagenetic reaction rates in marine sediments. J. Mar. Res. 56 (4), 905–936. https://doi.org/10.1357/002224098321667413.

Anderson, T.F., Raiswell, R., 2004. Sources and mechanisms for the enrichments of highly reactive iron in euxinic Black Sea sediments. Am. J. Sci. 304 (3), 203–233.

APHA, 2005. Standard methods for the examination of water and wastewater. pp. 1469. https://doi.org/10.2105/AJPH.51.6.940-a.

Arthur, M.A., Dean, W.E., 1998. Organic-matter production and preservation and evolution of anoxia in the Holocene Black Sea. Paleoceanography 13 (4), 395–411. https://doi.org/10.1029/98PA01161.

Berelson, W., et al., 2003. A time series of benthic flux measurements from Monterey Bay, CA. Cont. Shelf Res. 23 (5), 457–481. https://doi.org/10.1016/S0278-4343(03)00009-8.

Berner, R.A., 1970. Sedimentary pyrite formation. Am. J. Sci. 268 (1), 1–23. https://doi.org/10.2475/ajs.268.1.1.

Berner, R.A., 1984. Sedimentary pyrite formation: an update. Geochim. Cosmochim. Acta 48 (4), 605–615. https://doi.org/10.1016/0016-7037(84)90089-9.

Bodeanu, N., Moncheva, S., Ruta, G., Popa, L., 1998. Long-term evolution of the algal blooms in Romanian and Bulgarian Black Sea waters. Cercet. Mar. Rech. Mar. 31, 37–55.

Borsboom, M., et al., 1998. The Dutch-Belgian beamline at the ESRF. J. Synchrotron Radiat. 5 (3), 518–520. https://doi.org/10.1107/S0909049597013484.

Boudreau, B.P., 1984. On the equivalence of nonlocal and radial-diffusion models for porewater irrigation. J. Mar. Res. 42 (3), 731–735.

Boudreau, B.P., 1996. A method-of-lines code for carbon and nutrient diagenesis in aquatic sediments. Comput. Geosci. 22 (5), 479–496. https://doi.org/10.1016/0098-3004(95)00115-8.

Boudreau, B.P., 1997. Diagenetic Models and their Implementation. Modelling Transport and Reactions in Aquatic Sediments. vol. 171. pp. 49–66. https://doi.org/10.I007/97S-3-642-60421-S.

Boudreau, B.P., 1998. Mean mixed depth of sediments: the wherefore and the why. Limnol. Oceanogr. 43 (3), 524–526. https://doi.org/10.4319/lo.1998.43.3.0524.

Boyd, P.W., Ellwood, M.J., 2010. The biogeochemical cycle of iron in the ocean. Nat. Geosci. 3 (10), 675–682. https://doi.org/10.1038/ngeo964.

Burdige, D.J., 2006. Geochemistry of Marine Sediments. pp. 208–209. https://doi.org/10.1086/533614.

Burton, E.D., Bush, R.T., Sullivan, L.A., 2006. Fractionation and extractability of sulfur, iron and trace elements in sulfidic sediments. Chemosphere 64 (8), 1421–1428. https://doi.org/10.1016/j.chemosphere.2005.12.003.

Burton, E.D., Sullivan, L.A., Bush, R.T., Johnston, S.G., Keene, A.F., 2008. A simple and inexpensive chromium-reducible sulfur method for acid-sulfate soils. Appl. Geochem. 23 (9), 2759–2766. https://doi.org/10.1016/j.apgeochem.2008.07.007.

Canfield, D.E., 1989. Reactive iron in marine sediments. Geochim. Cosmochim. Acta 53 (3), 619–632. https://doi.org/10.1016/0016-7037(89)90005-7.

Canfield, D.E., Thamdrup, B., Hansen, J.W., 1993. The anaerobic degradation of organic matter in Danish coastal sediments: iron reduction, manganese reduction, and sulfate reduction. Geochim. Cosmochim. Acta 57 (16), 3867–3883. https://doi.org/10.1016/0016-7037(93)90340-3.

Canfield, D.E., Lyons, T.W., Raiswell, R., 1996. A model for iron deposition to euxinic Black Sea sediments. Am. J. Sci. 296 (7), 818–834. https://doi.org/10.2475/ajs.296.7.818.

Capet, A., Beckers, J.M., Grégoire, M., 2013. Drivers, mechanisms and long-term variability of seasonal hypoxia on the Black Sea northwestern shelf - is there any recovery after eutrophication? Biogeosciences 10 (6), 3943–3962. https://doi.org/10.5194/bg-10-3943-2013.

Capet, A., Stanev, E.V., Beckers, J.M., Murray, J.W., Grégoire, M., 2016. Decline of the Black Sea oxygen inventory. Biogeosciences 13 (4), 1287–1297. https://doi.org/10.5194/bg-13-1287-2016.

Claff, S.R., Sullivan, L.A., Burton, E.D., Bush, R.T., 2010. A sequential extraction procedure for acid sulfate soils: partitioning of iron. Geoderma 155 (3-4), 224–230. https://doi.org/10.1016/j.geoderma.2009.12.002.

Conway, T.M., John, S.G., 2014. Quantification of dissolved iron sources to the North Atlantic Ocean. Nature 511 (7508), 212–215. https://doi.org/10.1038/nature13482.

Coolen, M.J.L., Saenz, J.P., Giosan, L., Trowbridge, N.Y., Dimitrov, P., Dimitrov, D., Eglinton, T.I., 2009. DNA and lipid molecular stratigraphic records of haptophyte succession in the Black Sea during the Holocene. Earth Planet. Sci. Lett. 284 (3-4), 610–621. https://doi.org/10.1016/j.epsl.2009.05.029.

Cullen, J.T., Chong, M., Ianson, D., 2009. GB4012 British Columbian continental shelf as a source of dissolved iron to the subarctic northeast Pacific Ocean. Glob. Biogeochem. Cycles 23 (4). https://doi.org/10.1029/2008GB003326.

Dale, A.W., Nickelsen, L., Scholz, F., Hensen, C., Oschlies, A., Wallmann, K., 2015. A revised global estimate of dissolved iron fluxes from marine sediments. Glob. Biogeochem. Cycles 29 (5), 691–707. https://doi.org/10.1002/2014GB005017.

De Baar, H.J.W., et al., 2008. Titan: a new facility for ultraclean sampling of trace elements and isotopes in the deep oceans in the international Geotraces program. Mar. Chem. 111 (1-2), 4–21. https://doi.org/10.1016/j.marchem.2007.07.009.

Diaz, R.J., Rosenberg, R., 1995. Marine benthic hypoxia: a review of its ecological effects and the behavioural responses of benthic macrofauna. Oceanogr. Mar. Biol. Annu. Rev. 33, 245–303.

Diaz, R.J., Rosenberg, R., 2008. Spreading dead zones and consequences for marine ecosystems. Science 321 (5891), 926–929. https://doi.org/10.1126/science.1156401.

Eckert, S., Brumsack, H.J., Severmann, S., Schnetger, B., März, C., Fröllje, H., 2013. Establishment of euxinic conditions in the Holocene Black Sea. Geology 41 (4), 431–434. https://doi.org/10.1130/G33826.1.

Eleftheriou, A., McIntyre, A., 2007. Methods for the Study of Marine Benthos: Third Edition. pp. 1–418. https://doi.org/10.1002/9780470995129.

Elrod, V.A., Berelson, W.M., Coale, K.H., Johnson, K.S., 2004. The flux of iron from continental shelf sediments: a missing source for global budgets. Geophys. Res. Lett. 31 (12), 2–5. https://doi.org/10.1029/2004GL020216.

Emerson, S., Jahnke, R., Heggie, D., 1984. Sediment-water exchange in shallow water estuarine sediments. J. Mar. Res. 42 (3), 709–730. https://doi.org/10.1357/002224084788505942.

Friedl, G., Dinkel, C., Wehrli, B., 1998. Benthic fluxes of nutrients in the northwestern Black Sea. Mar. Chem. 62 (1-2), 77–88. https://doi.org/10.1016/S0304-4203(98)00029-2.

Friedrich, J., Dinkel, C., Friedl, G., Pimenov, N., Wijsman, J., Gomoiu, M.-T., Cociasu, A., Popa, L., Wehrli, B., 2002. Benthic nutrient cycling and diagenetic pathways in the North-western Black Sea. Estuar. Coast. Shelf Sci. 54 (3), 369–383. https://doi.org/10.1006/ecss.2000.0653.

Gerringa, L.J.A., Rijkenberg, M.J.A., Bown, J., Margolin, A.R., Laan, P., de Baar, H.J.W., 2016. Fe-binding dissolved organic ligands in the oxic and suboxic waters of the Black Sea. Front. Mar. Sci. 3. https://doi.org/10.3389/fmars.2016.00084.

Gledhill, M., van den Berg, C.M.G., 1994. Determination of complexation of iron(III) with natural organic complexing ligands in seawater using cathodic stripping voltammetry. Mar. Chem. 47 (1), 41–54. https://doi.org/10.1016/0304-4203(94)90012-4.

Henkel, S., Kasten, S., Poulton, S.W., Staubwasser, M., 2016. Determination of the stable iron isotopic composition of sequentially leached iron phases in marine sediments. Chem. Geol. https://doi.org/10.1016/j.chemgeo.2015.12.003.

Homoky, W.B., Hembury, D.J., Hepburn, L.E., Mills, R.A., Statham, P.J., Fones, G.R., Palmer, M.R., 2011. Iron and manganese diagenesis in deep sea volcanogenic sediments and the origins of pore water colloids. Geochim. Cosmochim. Acta 75 (17), 5032–5048. https://doi.org/10.1016/j.gca.2011.06.019.

Hong, H., Kester, D.R., 1986. Redox state of iron in the offshore waters of Peru. Limnol. Oceanogr. 31 (3), 612–626. https://doi.org/10.4319/lo.1986.31.3.0612.

Hoving, A.L., Sander, M., Bruggeman, C., Behrends, T., 2017. Redox properties of clay-rich sediments as assessed by mediated electrochemical analysis: separating pyrite, siderite and structural Fe in clay minerals. Chem. Geol. https://doi.org/10.1016/j.chemgeo.2017.03.022.

Johnson, K., Elrod, V., Fitzwater, S., 2007. Developing standards for dissolved iron in seawater. Eos 88 (11), 131–132. https://doi.org/10.1029/2007EO110003.

Jørgensen, B.B., 1977. The sulfur cycle of a coastal marine sediment (Limfjorden, Denmark). Limnol. Oceanogr. 22 (5), 814–832. https://doi.org/10.4319/lo.1977.22.5.0814.

Kappler, A., Schink, B., Newman, D.K., 2005. Fe(III) mineral formation and cell encrustation by the nitrate-dependent Fe(II)-oxidizer strain BoFeN1. Geobiology 3 (4), 235–245. https://doi.org/10.1111/j.1472-4669.2006.00056.x.

Klar, J.K., et al., 2017. Stability of dissolved and soluble Fe (II) in shelf sediment pore waters and release to an oxic water column. Biogeochemistry 135 (1-2), 49–67.

Klunder, M.B., Laan, P., Middag, R., De Baar, H.J.W., van Ooijen, J.C., 2011. Dissolved iron in the Southern Ocean (Atlantic sector). Deep-Sea Res. II Top. Stud. Oceanogr. 58 (25-26), 2678–2694. https://doi.org/10.1016/j.dsr2.2010.10.042.

Kraal, P., Dijkstra, N., Behrends, T., Slomp, C.P., 2017. Phosphorus burial in sediments of the sulfidic deep Black Sea: key roles for adsorption by calcium carbonate and apatite authigenesis. Geochim. Cosmochim. Acta 204, 140–158. https://doi.org/10.1016/j.gca.2017.01.042.

Lam, P.J., Ohnemus, D.C., Marcus, M.A., 2012. The speciation of marine particulate iron adjacent to active and passive continental margins. Geochim. Cosmochim. Acta 80, 108–124. https://doi.org/10.1016/j.gca.2011.11.044.

Lenz, C., Jilbert, T., Conley, D.J., Slomp, C.P., 2015. Hypoxia-driven variations in iron and manganese shuttling in the Baltic Sea over the past 8 kyr. Geochem. Geophys. Geosyst. 16 (10), 3754–3766. https://doi.org/10.1002/2015GC005960.

Levin, L.A., Ekau, W., Gooday, A.J., Jorissen, F., Middelburg, J.J., Naqvi, S.W.A., Neira, C., Rabalais, N.N., Zhang, J., 2009. Effects of natural and human-induced hypoxia on coastal benthos. Biogeosciences 6 (10), 2063–2098. https://doi.org/10.5194/bg-6-2063-2009.

Lovley, D.R., Phillips, E.J., 1987. Rapid assay for microbially reducible ferric iron in aquatic sediments. Appl. Environ. Microbiol. 53 (7), 1536–1540. https://doi.org/10.1007/BF01611203.
Lyons, T.W., Severmann, S., 2006. A critical look at iron paleoredox proxies: new insights from modern euxinic marine basins. Geochim. Cosmochim. Acta 70 (23 SPEC. ISS.), 5698–5722. https://doi.org/10.1016/j.gca.2006.08.021.
Martin, J.H., Fitzwater, S.E., 1988. Iron Deficiency Limits Phytoplankton Growth in the North-East Pacific Subarctic. https://doi.org/10.1038/331341a0.
Martin, W.R., Banta, G.T., 1992. The measurement of sediment irrigation rates: a comparison of the Br tracer and 222-Rn/ 226-Ra disequilibrium techniques. J. Mar. Res. 50 (1), 125–154. https://doi.org/10.1357/002224092784797737.
Meile, C., Berg, P., Van Cappellen, P., Tuncay, K., 2005. Solute-specific pore water irrigation: implications for chemical cycling in early diagenesis. J. Mar. Res. 63, 601–621. https://doi.org/10.1357/0022240054307885.
Millero, F.J., Sotolongo, S., Izaguirre, M., 1987. The oxidation kinetics of Fe(II) in seawater. Geochim. Cosmochim. Acta 51 (4), 793–801. https://doi.org/10.1016/0016-7037(87)90093-7.
Moore, C.M., et al., 2013. Processes and patterns of oceanic nutrient limitation. Nat. Publ. Group 6 (9), 701–710. https://doi.org/10.1038/ngeo1765.
Murray, J.W., Jannasch, H.W., Honjo, S., Anderson, R.F., Reeburgh, W.S., Top, Z., Friederich, G.E., Codispoti, L.A., Izdar, E., 1989. Unexpected changes in the oxic/anoxic interface in the Black Sea. Nature 338 (6214), 411–413. https://doi.org/10.1038/338411a0.
Nealson, K.H., 1997. Sediment bacteria: who's there, what are they doing, and what's new? Annu. Rev. Earth Planet. Sci. 25, 403–434. https://doi.org/10.1146/annurev.earth.25.1.403.
Nikitenko, S., et al., 2008. Implementation of a combined SAXS/WAXS/QEXAFS set-up for time-resolved in situ experiments. J. Synchrotron Radiat. 15 (6), 632–640. https://doi.org/10.1107/S0909049508023327.
Noble, A.E., et al., 2012. Basin-scale inputs of cobalt, iron, and manganese from the Benguela-Angola front to the South Atlantic Ocean. Limnol. Oceanogr. 57 (4), 989–1010. https://doi.org/10.4319/lo.2012.57.4.0989.
Noffke, A., Hensen, C., Sommer, S., Scholz, F., Bohlen, L., Mosch, T., Graco, M., Wallmann, K., 2012. Benthic iron and phosphorus fluxes across the Peruvian oxygen minimum zone. Limnol. Oceanogr. 57 (3), 851–867. https://doi.org/10.4319/lo.2012.57.3.0851.
Pakhomova, S.V., Hall, P.O.J., Kononets, M.Y., Rozanov, A.G., Tengberg, A., Vershinin, A.V., 2007. Fluxes of iron and manganese across the sediment-water interface under various redox conditions. Mar. Chem. 107 (3), 319–331. https://doi.org/10.1016/j.marchem.2007.06.001.
Panin, N., Jipa, D., 2002. Danube river sediment input and its interaction with the North-western Black Sea. Estuar. Coast. Shelf Sci. 54, 551–562 doi:10.1006.
Pollard, R.T., et al., 2009. Southern Ocean deep-water carbon export enhanced by natural iron fertilization. Nature 457 (7229), 577–580. https://doi.org/10.1038/nature07716.
Popa, A., 1993. Liquid and Sediment Inputs of the Danube River into the North-Western Black Sea. Transport of carbon and nutrients in lakes and estuaries, (Part 6). pp. 137–149.
Postma, D., 1985. Concentration of Mn and separation from Fe in sediments-I. Kinetics and stoichiometry of the reaction between birnessite and dissolved Fe(II) at 10 degrees C. Geochim. Cosmochim. Acta 49 (4), 1023–1033. https://doi.org/10.1016/0016-7037(85)90316-3.
Poulton, S.W., Canfield, D.E., 2005. Development of a sequential extraction procedure for iron: implications for iron partitioning in continentally derived particulates. Chem. Geol. 214 (3-4), 209–221. https://doi.org/10.1016/j.chemgeo.2004.09.003.
Poulton, S.W., Raiswell, R., 2002. The low-temperature geochemical cycle of iron: from continental fluxes to marine sediment deposition. Am. J. Sci. 302 (9), 774–805. https://doi.org/10.2475/ajs.302.9.774.
Raiswell, R., Berner, R.A., 1985. Pyrite formation in euxinic and semi-euxinic sediments. Am. J. Sci. 285 (8), 710–724. https://doi.org/10.2475/ajs.285.8.710.
Raiswell, R., Buckley, F., Berner, R.A., 1988. Degree of pyritization of iron as a paleoenvironmental indicator of bottom-water oxygenation. SEPM J. Sediment. Res. 58. https://doi.org/10.1306/212F8E72-2B24-11D7-8648000102C1865D.
Raiswell, R., Canfield, D.E., 2012. The iron biogeochemical cycle past and present. Geochem. Perspect. 1 (1), 1–220. https://doi.org/10.7185/geochempersp.1.1.
Raiswell, R., Vu, H.P., Brinza, L., Benning, L.G., 2010. The determination of labile Fe in ferrihydrite by ascorbic acid extraction: methodology, dissolution kinetics and loss of solubility with age and de-watering. Chem. Geol. 278 (1-2), 70–79. https://doi.org/10.1016/j.chemgeo.2010.09.002.
Ravel, B., Newville, M., 2005. ATHENA, ARTEMIS, HEPHAESTUS: data analysis for X-ray absorption spectroscopy using IFEFFIT. J. Synchrotron Radiat. 12 (4), 537–541. https://doi.org/10.1107/S0909049505012719.
Rijkenberg, M.J.A., de Baar, H.J.W., Bakker, K., Gerringa, L.J.A., Keijzer, E., Laan, M., Laan, P., Middag, R., Ober, S., van Ooijen, J., Ossebaar, S., van Weerlee, E.M., Smit, M.G., 2015. "PRISTINE", a new high volume sampler for ultraclean sampling of trace metals and isotopes. Mar. Chem. 177, 501–509. https://doi.org/10.1016/j.marchem.2015.07.001.
Rijkenberg, M.J.A., et al., 2014. The distribution of dissolved iron in the West Atlantic Ocean. PLoS ONE 9 (6), 1–14. https://doi.org/10.1371/journal.pone.0101323.
Robertson, E.K., Roberts, K.L., Burdorf, L.D.W., Cook, P., Thamdrup, B., 2016. Dissimilatory nitrate reduction to ammonium coupled to Fe(II) oxidation in sediments of a periodically hypoxic estuary. Limnol. Oceanogr. 61 (1), 365–381. https://doi.org/10.1002/lno.10220.
Rue, E.L., Bruland, K.W., 1995. Complexation of iron(III) by natural organic ligands in the Central North Pacific as determined by a new competitive ligand equilibration/adsorptive cathodic stripping voltammetric method. Mar. Chem. 50 (1-4), 117–138. https://doi.org/10.1016/0304-4203(95)00031-L.
Salomé, M., et al., 2013. The ID21 scanning X-ray microscope at ESRF. J. Phys. Conf. Ser. 425. https://doi.org/10.1088/1742-6596/425/18/182004.
Schlitzer, R., 2015. Ocean Data View. 2012. Available: http://odv.awi.de Accepted on October.
Schlüter, M., Sauter, E., Hansen, H.P., Suess, E., 2000. Seasonal variations of bioirrigation in coastal sediments: modelling of field data. Geochim. Cosmochim. Acta 64 (5), 821–834. https://doi.org/10.1016/S0016-7037(99)00375-0.
Scholz, F., Loscher, C.R., Fiskal, A., Sommer, S., Hensen, C., Lomnitz, U., Wuttig, K., Gottlicher, J., Kossel, E., Steininger, R., Canfield, D.E., 2016. Nitrate-dependent iron oxidation limits iron transport in anoxic ocean regions. Earth Planet. Sci. Lett. https://doi.org/10.1016/j.epsl.2016.09.025.
Scholz, F., McManus, J., Mix, A.C., Hensen, C., Schneider, R.R., 2014a. The impact of ocean deoxygenation on iron release from continental margin sediments. Nat. Geosci. 7 (May), 433–437. https://doi.org/10.1038/ngeo2162.
Scholz, F., Severmann, S., McManus, J., Hensen, C., 2014b. Beyond the Black Sea paradigm: the sedimentary fingerprint of an open-marine iron shuttle. Geochim. Cosmochim. Acta. https://doi.org/10.1016/j.gca.2013.11.041.
Schwertmann, U., Cornell, R.M., 2007. Frontmatter. In: Iron Oxides in the Laboratory, https://doi.org/10.1002/9783527613229.fmatter. i–xviii.
Severmann, S., McManus, J., Berelson, W.M., Hammond, D.E., 2010. The continental shelf benthic iron flux and its isotope composition. Geochim. Cosmochim. Acta 74 (14), 3984–4004. https://doi.org/10.1016/j.gca.2010.04.022.
Sinninghe Damsté, J.S., Wakeham, S.G., Kohnen, M.E.L., Hayes, J.M., de Leeuw, J.W., 1993. A 6000 year sedimentary molecular record of chemocline excursions in the Black Sea. Nature 362 (6423), 827–829. https://doi.org/10.1038/362827a0.
Slomp, C.P., Malschaert, J.F.P., Lohse, L., Van Raaphorst, W., 1997. Iron and manganese cycling in different sedimentary environments on the North Sea continental margin. Cont. Shelf Res. 17 (9), 1083–1117. https://doi.org/10.1016/S0278-4343(97)00005-8.
Slomp, C.P., Mort, H.P., Jilbert, T., Reed, D.C., Gustafsson, B.G., Wolthers, M., 2013. Coupled dynamics of iron and phosphorus in sediments of an oligotrophic coastal basin and the impact of anaerobic oxidation of methane. PLoS ONE 8 (4). https://doi.org/10.1371/journal.pone.0062386.
Soetaert, K., Petzoldt, T., Meysman, F.J.R., 2010. Marelac: Tools for Aquatic Sciences v2.1.3. R package. .
Tagliabue, A., Bowie, A. R., Boyd, P. W., Buck, K. N., Johnson, K. S., Saito, M. A., 2017. The integral role of iron in ocean biogeochemistry. 10.1038/nature21058.
Tankéré, S.P.C., Muller, F.L.L., Burton, J.D., Statham, P.J., Guieu, C., Martin, J.M., 2001. Trace metal distributions in shelf waters of the northwestern Black Sea. Cont. Shelf Res. 21 (13-14), 1501–1532. https://doi.org/10.1016/S0278-4343(01)00013-9.
Van Santvoort, P.J., De Lange, G.J., Thomson, J., Colley, S., Meysman, F.J., Slomp, C.P., 2002. Oxidation and origin of organic matter in surficial Eastern Mediterranean hemipelagic sediments. Aquat. Geochem. 8 (3), 153–175. https://doi.org/10.1023/A:1024271706896.
Vink, S., 2001. Dissolved Fe in the upper waters of the Pacific sector of the Southern Ocean. Deep-Sea Res. II Top. Stud. Oceanogr. 48 (19-20), 3913–3941.
Weber, A., Riess, W., Wenzhoefer, F., Jørgensen, B.B., 2001. Sulfate reduction in Black Sea sediments: in situ and laboratory radiotracer measurements from the shelf to 2000 m depth. Deep-Sea Res. I Oceanogr. Res. Pap. 48 (9), 2073–2096. https://doi.org/10.1016/S0967-0637(01)00006-1.
Wijsman, J.W.M., Herman, P.M.J., Gomoiu, M.T., 1999. Spatial distribution in sediment characteristics and benthic activity on the northwestern Black Sea shelf. Mar. Ecol. Prog. Ser. 181, 25–39. https://doi.org/10.3354/meps181025.
Wijsman, J.W.M., Herman, P.M.J., Middelburg, J.J., Soetaert, K., 2002. A model for early diagenetic processes in sediments of the continental shelf of the Black Sea. Estuar. Coast. Shelf Sci. 54 (may), 403–421. https://doi.org/10.1006/ecss.2000.0655.
Wijsman, J.W.M., Middelburg, J.J., Heip, C.H.R., 2001a. Reactive iron in Black Sea sediments: implications for iron cycling. Mar. Geol. 172 (3-4), 167–180. https://doi.org/10.1016/S0025-3227(00)00122-5.
Wijsman, J.W.M., Middelburg, J.J., Herman, P.M.J., Böttcher, M.E., Heip, C.H.R., 2001b. Sulfur and iron speciation in surface sediments along the northwestern margin of the Black Sea. Mar. Chem. 74 (4), 261–278. https://doi.org/10.1016/S0304-4203(01)00019-6.
Witbaard, R., Duineveld, G.C.A., Van der Weele, J.A., Berghuis, E.M., Reyss, J.P., 2000. The benthic response to the seasonal deposition of phytopigments at the Porcupine Abyssal Plain in the North East Atlantic. J. Sea Res. 43 (1), 15–31. https://doi.org/10.1016/S1385-1101(99)00040-4.
Wu, J., Boyle, E., Sunda, W., Wen, L.S., 2001. Soluble and colloidal iron in the oligotrophic North Atlantic and North Pacific. Science 293 (5531), 847–849. https://doi.org/10.1126/science.1059251.